ISSN 0029-3865

CBPF- CENTRO BRASILEIRO DE PESQUISAS FÍSICAS

Notas de Física

CBPF-NF-039/93

Potts Antiferromagnet on a Family of Fractal Lattices: Exact Results for an Unusual Phase

by

J.A. Redinz, A.C.N. de Magalhães and E.M.F. Curado

Rio de Janeiro
1993

Abstract

The three-state antiferromagnetic Potts model on a family of bipartite diamond hierarchical lattices is investigated. We prove that the correlations have a power law and that the order parameter vanishes in the entire low-temperature phase as predicted by Berker and Kadanoff. The internal energy, specific heat and entropy as functions of temperature are also exactly calculated. It is shown that the local order parameter has two distinct multifractal structures : one at the critical point and another at the unusual phase.

KEY-WORDS : Potts Model, Antiferromagnet, Fractal Lattice, Multifractal

PACS NUMBERS : 64.60.Ak, 75.10.Hk, 64.60.Cn

1 Introduction

Although the majority of macroscopic physical systems and statistical mechanics models obey the third law of thermodynamics, there are notable exceptions like, for example, the substances [1] ice, carbon monoxide and nitrous oxide, some frustrated systems (e.g. Ising antiferromagnet on the triangular lattice [2], spin glasses [3]), some Potts antiferromagnets [4] and some other classical discrete spin systems [5]. The study of statistical properties of such systems is much more complex due to their infinite macroscopic ground state degeneracy. In particular, Berker and Kadanoff [6] suggested, using a one-parameter renormalization group (RG) argument, that systems with finite residual (i.e. at null temperature) entropy per particle may present a distinctive low temperature phase with no obvious order parameter and with a power law decay of correlations. In fact, they obtained, within a Migdal-Kadanoff RG approximation, such unusual phase in the q-state ($q > 2$) antiferromagnetic (AF) Potts model on d-dimensional hypercubic lattices whenever $d > d_c(q)$, where $d_c(q)$ is the lower critical dimension for fixed q below which there is no phase transition. However Rácz and Vicsek [7] argued that the appearance of the distinctive phase could be an artifact of the one-parameter RG treatment. Since then, much work

has been done looking for this phase in the AF Potts model on different Bravais (see, for example, [8] and references therein) and fractal lattices [9,10,11,12]. In particular, many approximate calculations (see [8] and references therein) for the $q = 3$ case on the bipartite cubic lattice indicate a continuous transition at $T_c \neq 0$ from the paramagnetic to the long-range ordered BSS (broken sublattice symmetry) phase. The latter is characterized by the predominance of one of the states in one sublattice and of the other two states (randomly distributed with equal probabilities) on the other sublattice. Excluding Ono's simulations [13] (which, according to [8], have an insufficient number of Monte Carlo steps) and some indications for the divergence of the correlation length below T_c despite the nonzero order parameter [8], there has not been found any evidence for the unusual phase in the three-dimensional $q = 3$ case or for any value of q on a number of Bravais lattices. On the other hand, the same is not true for some fractal lattices, where this phase has been established by either exact RG transformations [11,12] or by the Migdal-Kadanoff RG approximation [9,10]. It is worth mentioning that the exact results of [12] show that the distinctive phase is neither an artifact of a one parameter RG treatment nor an artifact of the Migdal-Kadanoff bond-moving procedure and can, therefore, occur in a lattice which is not a combination of series and/or paralell bonds. The

unusual phase was detected in the RG procedures [9,10,11,12] through an attractor at a nonvanishing temperature — a feature which appears also in the RG framework of Berker and Kadanoff [6]. Furthermore, it was also proved [12], for the Ising case, that the correlations decay algebraically with distance along the whole unusual phase. But a detailed study of this phase including the exact temperature dependence of the order parameter and other thermodynamical quantities has not, as far as we know, been reported in the literature.

Herein we consider the 3-state AF Potts model on a family of diamond hierarchical lattice (HL) types which belongs to a bigger family of HL's on which the Potts antiferromagnet presents [11] the distinctive phase. Using an exact recursive procedure [14]-[17], we prove that the order parameter vanishes for all temperatures and that the local magnetization distribution has a multifractal structure at the critical point different from that along the unusual phase. We also calculate exactly the average internal energy, the specific heat and the entropy per spin as functions of temperature.

The outline of this paper is as follows. In Section 2 we define the model and the family of HL's to be considered herein. In Section 3 we prove that this family of systems has a low temperature phase with a power law decay of correlations. In Section 4 we derive the recursive relations for local

average quantities whose iteration leads to multifractal local magnetization profiles. In Section 5 we calculate, in an exact way, the order parameter, the internal energy, the specific heat and the entropy. Finally, the conclusions are given in Section 6.

2 Model

Qin and Yang [11] considered the q-state AF Potts model on the fractal family of diamond HL types whose generator is constituted by P branches in paralell, each of which has L bonds in series. They showed that, for an odd L and for $2 < q < q_c$ (where q_c is a cutoff value of q which depends on P and L), there appears the type of phase predicted by Berker and Kadanoff. Herein we shall consider the simplest family of HL's (with a minimum number of L) of this bigger family on which the q-state (q being the minimum integer below q_c) AF Potts model presents the unusual phase. Its generator (or basic cell) contains $P \geq 10$ branches of $L = 3$ bonds in series (see graph $G^{(1)}$, for $P = 10$, in Fig. 1), and the HL is constructed as follows. We start with a bond between the roots R_A and R_B (see $G^{(0)}$, for $P = 10$, in Fig. 1) and, in the next level, we replace it by the generator and continue successively substituting each bond of a level by the basic

cell. In the thermodynamic limit ($n \to \infty$) this family of HL's has a fractal dimension [18] $d_f(P)$ given by

$$d_f(P) = \frac{\ln(3P)}{\ln 3} \qquad (P \geq 10) \quad , \tag{1}$$

in particular, $d_f(10) = 3.09\ldots$.

Notice that the considered HL family is bipartite, i.e., each HL can be divided into two interpenetrating sublattices $\mathcal{A}$ (represented by points in Fig. 1) and $\mathcal{B}$ (represented by squares in Fig. 1) such that any site of one sublattice has as nearest neighbors only sites of the other sublattice at any level. Furthermore, contrarily to what happens in the case of L=even, each point belongs always to a given sublattice independently of the level n.

At each site i of the HL with P branches ($P \geq 10$), we associate a Potts variable $\sigma_i = 0, 1, 2$ and consider the 3-state AF Potts model described by the following dimensionless Hamiltonian at the n-level :

$$\beta\mathcal{H}_n^{(P)} = -3K_n^{(P)} \sum_{(ij)} \delta(\sigma_i, \sigma_j) \qquad (\beta \equiv 1/k_B T \ , \ K_n^{(P)} \equiv \beta J_n^{(P)}) \quad . \tag{2}$$

where $J_n^{(P)} < 0$ is the AF coupling constant between nearest neighbor spins at the n-level of the HL with P branches, the sum is over all nearest neighbor pairs $\langle i, j \rangle$ of spins, $\delta(\sigma_i, \sigma_j)$ is the Kronecker delta function, and T is the absolute temperature.

3 The Distinctive Low Temperature Phase

Let us now prove that each system of the above mentioned family has an unusual phase where the pair correlation function obeys a power law decay. For this, we consider the RG transformation defined by the renormalization of the basic cell (see, for $P = 10$, $n = 1$ of Fig. 1) (with reduced coupling constant $K'^{(P)}$ between any pair of neighbor spins) into the single bond ($n = 0$ of Fig. 1) linking the two roots with an effective reduced coupling constant $K'^{(P)}$. The RG recursive equation is obtained by imposing that the trace of $\{\exp(-\beta\mathcal{H}_1(K'^{(P)}))\}$ over the internal spins (i.e., those different from the rooted ones) of $G^{(1)}$ is proportional to $\{\exp(-\beta\mathcal{H}_0(K'^{(P)}))\}$. This is equivalent to preserve the correlation function between σ_{RA} and σ_{RB} [19] and it leads to :

$$t'(t,P) = \frac{1-\left(\frac{1-t^2}{1+2t^2}\right)^P}{1+2\left(\frac{1-t^2}{1+2t^2}\right)^P} \quad . \tag{3}$$

where we have used, for convenience, the thermal transmissivity variable [20] defined by :

$$t(K') \equiv \frac{1-e^{-3K'}}{1+2e^{-3K'}} \quad . \tag{4}$$

Thus, if we fix P and t_n (the thermal transmissivity at the n-level), we can obtain the transmissivities at previous levels by iterating Eq. (3), namely, $t_{n-1} = t'(t_n)$, $t_{n-2} = t'(t_{n-1}) = t^{(2)}(t_n)$ and so on until $t_0 = t^{(n)}(t_n)$ which

corresponds to the equivalent transmissivity between the roots of the HL with P branches at the n-level [19]. It is worth mentioning that our RG transformation (Eq. (3)) is an exact one due to the recursive construction of each HL and to the fact that the symmetries of the ground state are preserved for this choice of cells [12].

The plots of t' versus t and their corresponding phase diagrams are shown for $P = 9$, $P = 10$ and $P = 27$ in Fig. 2. We can see from it the appearance of an unusual phase, for finite $P > P_c = 9.25\ldots$ (or equivalently for $d_f(P) > d_c = 3.025\ldots$), characterized by an attractor at a nonzero temperature $t_{AF}^{(P)}$ (for $P = 10$, $\frac{k_B T_{AF}^{(10)}}{3|J|} = 0.286\ldots$, or equivalently, $t_{AF}^{(10)} = -0.477\ldots$), in the temperature range $0 \leq \frac{k_B T}{3|J|} < \frac{k_B T_c^{(P)}}{3|J|}$ (or equivalently $-1/2 \leq t < t_c^{(P)}$). We shall use the index notation AF to designate the unusual phase, despite the fact that the staggered magnetization is null along this phase (as we will see in Section 5). For temperatures above $\frac{k_B T_c^{(P)}}{3|J|}$ (or $t_c^{(P)} < t \leq 0$) all points flow under successive RG iterations to the paramagnetic attractor $\frac{k_B T_p}{3|J|} \to \infty$ (or $t_p = 0$), defining thus the paramagnetic phase. In Fig. 3 it is shown the plots of the transmissivity $t_{AF}^{(P)}$ and the critical transmissivity $t_c^{(P)}$ versus the fractal dimension $d_f(P)$. Notice that, as d_f diminishes tending to d_c, the fixed points $t_{AF}^{(P)}$ and $t_c^{(P)}$ approach each other until they merge, for $d_f = d_c$, into a single marginal

one. Observe also that, for $d_f >> d_c$, the AF attractor converges to $T = 0$. These behaviors confirm those suggested by Berker and Kadanoff [6] and are similar to those obtained [12], in an exact way, for the $q = 2$ and 4-state AF Potts model on the m-sheet Sierpinski gasket with side $b = 4$.

The correlation length critical exponent $\nu^{(P)}$ can be determined by :

$$\nu^{(P)} = \frac{\ln L}{\ln r_c^{(P)}} \quad , \tag{5}$$

where L is the chemical distance between the roots of the basic cell ($L = 3$) and

$$r_c^{(P)} \equiv \left. \frac{dt'(t,P)}{dt} \right]_{t_c^{(P)}} \quad . \tag{6}$$

The plot of $\nu^{(P)}$ as function of $d_f(P)$ can be seen in Fig. 4. Similar to [12], $\nu^{(P)}$ diverges for $d_f = d_c$ as a power law, namely $\nu^{(P)} \sim [0.841\ldots](d_f(P) - d_c)^{-0.442\ldots}$ as d_f approaches d_c from above.

Let us now prove, through a procedure similar to [12], that the correlation function Γ_{AB} between the two roots of the HL with a finite number of P branches decays algebraically with distance along the unusual phase whose attractor occurs at $t_{AF}^{(P)}$. We define the correlation function between the roots of the HL at the n-level and at the temperature corresponding to the transmissivity t_n, $\Gamma_{AB}^{(n)}(t_n)$, by [21] :

$$\Gamma_{AB}^{(n)}(t_n) = \frac{3\langle \delta(\sigma_{RA}, \sigma_{RB}) \rangle_{n,P} - 1}{2} \quad . \tag{7}$$

where $(\ldots)_{n,P}$ means the thermal average taken at the n-level of a HL with P branches. On the other hand $\Gamma_{AB}^{(n)}(t_n)$ is related to the equivalent transmissivity between σ_{RA} and σ_{RB} through [22] :

$$\Gamma_{AB}^{(n)}(t_n) = t_n^{(n)} \equiv t^{(n)}(t_n) \quad , \tag{8}$$

where, as already pointed out, $t_n^{(n)}$ is the n^{th} iteration of Eq. (3) applied to t_n.

Expanding $t'(t_n)$ around the AF attractor we have

$$t'(t_n) \simeq t_{AF}^{(P)} + r_{AF}^{(P)}(t_n - t_{AF}^{(P)}) \qquad (t_n \simeq t_{AF}^{(P)}) \quad , \tag{9}$$

where $r_{AF}^{(P)} \equiv \frac{dt'(t,P)}{dt}\,|_{t_{AF}^{(P)}}$, $0 < r_{AF}^{(P)} < 1$. After n iterations of this equation we get

$$t_n^{(n)} = t_{AF}^{(P)} + (r_{AF}^{(P)})^n(t_n - t_{AF}^{(P)}) \qquad (t_n \simeq t_{AF}^{(P)}) \quad . \tag{10}$$

Combining (8) and (10) we obtain, in the fractal limit ($n \to \infty$),

$$\Gamma_{AB} \equiv \left[\Gamma_{AB}^{(n)}(t_n) - \Gamma_{AB}^{(\infty)}(t_\infty)\right] \sim (r_{AF}^{(P)})^n(t_n - t_{AF}^{(P)}) \sim L_n^{-\epsilon^{(P)}} \tag{11}$$

with

$$\epsilon^{(P)} \equiv -\frac{\ln r_{AF}^{(P)}}{\ln 3} \quad , \tag{12}$$

where L_n is the chemical distance between the roots of the HL ($L_n = 3^n$). This result is in agreement with the suggestion of power-law decay made by Berker and Kadanoff [6] .

Assuming that, similar to the asymptotic behavior of $\Gamma_{AB}(L_{AB} \to \infty)$ in the d-dimensional Bravais lattices,

$$\Gamma_{AB}(L_{AB}) \sim L_{AB}^{-(d_f-2+\eta_{AF})} \qquad (L_{AB} \to \infty) \tag{13}$$

we obtain η_{AF} versus $d_f(P)$ as shown in Fig. 4 by triangles, which is similar to that found in [12]. It is worth emphasizing that this η_{AF} exponent is valid for the whole unusual phase ($-1/2 \leq t < t_c^{(P)}$), but not necessarily for $t = t_c^{(P)}$ (see Section 5.2).

4 Local Average Quantities

In order to characterize better this unusual phase, we shall calculate in an exact way the order parameter and other thermodynamical quantities as well. For this, we shall use a recursive method developed initially for Ising models [14,15,16] and, afterwards, extended to the Potts model [17] on HL's. This technique allows one to obtain exact recursive relations for local average quantities, from which one can derive global thermodynamical functions such as the order parameter, the internal energy and the specific heat. Let us, in this section, focus on the calculation of local average quantities.

4.1 Recursive Relations

Let us now explain the general idea of the recursive method [17]. First, we consider the graph $G^{(n)}$ (i.e. the HL with P branches at the n-level) as composed of two subgraphs $G_1^{(n)}$ and $G_2^{(n)}$ which intersect at the sites with spins μ_1 and μ_2 created at previous levels (see Fig. 5); one of them being necessarily aggregated at the $(n-1)$ level. The graph $G_1^{(n)}$ contains, besides μ_1 and μ_2, the spins σ_1 and σ_2 which are aggregated at the n-level; the remaining spins belong to $G_2^{(n)}$. We, then, fix the rooted spin σ_{RA} at the state 0 in order to break the symmetry between the thermodynamical configurations. The next step consists in replacing $G_2^{(n)}$ by an effective bond $G_{ef}^{(n)}$ linking μ_1 and μ_2 (see Fig. 5(b)) whose effective dimensionless Hamiltonian $\mathcal{H}_{ef}^{(n)}$ is given by :

$$\begin{aligned} \beta\mathcal{H}_{ef}^{(n)} &= -3\left[h_1^{(n)}\delta(\mu_1,0) + h_2^{(n)}\delta(\mu_2,0) + K_E^{(n)}\delta(\mu_1,\mu_2) + \right. \\ &+ \left. K_S^{(n)}\delta(\mu_1,0)\delta(\mu_2,0) + C^{(n)}\right] \qquad . \end{aligned} \tag{14}$$

In Eq. (14), $h_1^{(n)}$ and $h_2^{(n)}$ are effective fields acting on the respective spins μ_1 and μ_2 induced by the above break of symmetry. The parameter $K_E^{(n)}$ is an effective coupling between μ_1 and μ_2 due to the remaining spins of $G_2^{(n)}$ and $K_S^{(n)}$ is another effective coupling which acts on μ_1 and μ_2 only when they are both in the same state as σ_{RA}. $C^{(n)}$ is a constant originated

from the renormalization of the energy. Once we have introduced $G_{ef}^{(n)}$, we calculate two separate sets S_1 and S_2 of local average quantities in terms of the coupling constant K_n and of the effective parameters $h_1^{(n)}$, $h_2^{(n)}$, $K_E^{(n)}$, $K_S^{(n)}$ and $C^{(n)}$. The set S_1 contains thermal averages of local quantities involving only the spins μ_1 and/or μ_2, and the set S_2 refers to averages which contain the spins σ_1 and/or σ_2. From the set S_1, we obtain the effective parameters as functions of its constituents averages and of K_n. Finally, the replacement of the effective parameters by these functions in S_2 provides local average quantities involving the spins generated at the n-level in terms of averages containing spins generated at previous levels of the HL with P branches.

We obtain, thus, the following system of coupled equations :

$$\begin{aligned}
m_{\sigma_1}^{(n)} &= a_n m_{\mu_2}^{(l)} + b_n m_{\mu_1}^{(l)} + c_n \Delta_{\mu_1\mu_2}^{(n-1)} \\
m_{\sigma_2}^{(n)} &= a_n m_{\mu_1}^{(l)} + b_n m_{\mu_2}^{(l)} + c_n \Delta_{\mu_1\mu_2}^{(n-1)} \\
\Delta_{\mu_1\sigma_2}^{(n)} &= (1 + 2a_n - b_n) m_{\mu_2}^{(l)} + (b_n + 2c_n) \Delta_{\mu_1\mu_2}^{(n-1)} \\
\Delta_{\sigma_1\sigma_2}^{(n)} &= (a_n + b_n)(m_{\mu_1}^{(l)} + m_{\mu_2}^{(l)}) + d_n \Delta_{\mu_1\mu_2}^{(n-1)} \\
\Delta_{\mu_2\sigma_1}^{(n)} &= (1 + 2a_n - b_n) m_{\mu_2}^{(l)} + (b_n + 2c_n) \Delta_{\mu_1\mu_2}^{(n-1)} \qquad (l < n) \quad ,
\end{aligned} \tag{15}$$

where we chose to define the local magnetization $m_i^{(k)}$ at site i of the k-level

HL with P branches by

$$m_i^{(k)} \equiv \langle \delta(\sigma_i, 0) \rangle_{k,P} - 1/3 \tag{16}$$

without the normalization factor 3/2 since it leads (as we will see in Section 5.1) to a normalized order parameter. The function $\Delta_{ij}^{(k)}$, a kind of correlation function which appears in this technique as a natural variable in the case of the q-state Potts model (for $q \neq 2$) [17], is defined by

$$\Delta_{ij}^{(k)} \equiv 3\langle \delta(\sigma_i, 0)\delta(\sigma_j, 0) \rangle_{k,P} - \langle \delta(\sigma_i, \sigma_j) \rangle_{k,P} \tag{17}$$

In Eq. (15), the coefficients a_n, b_n, c_n and d_n are functions of the coupling constant $K_n^{(P)}$ at the n-level of the HL with P branches which are given, expressed in terms of the transmissivity t_n, by :

$$\begin{aligned} a_n &\equiv \frac{t_n(1+t_n)}{1+t_n+t_n^2} & b_n &\equiv \frac{t_n^2}{1+t_n+t_n^2} \\ c_n &\equiv \frac{t_n^3(1-t_n^2)}{(1+2t_n^3)(1+t_n+t_n^2)} & d_n &\equiv \frac{t_n^2(1+3t_n+t_n^2-2t_n^3)}{(1+2t_n^3)(1+t_n+t_n^2)} \end{aligned} \tag{18}$$

where the set $\{t_n, t_{n-1}, \ldots, t_0\}$ can be obtained from $t_{n-1} = t'(t_n)$ with $t'(t, P)$ given by Eq. (3).

Besides the coupled equations (15), we also have the following recurrent relation (which will be used in the calculation of the internal energy in the

next section) :

$$\langle\delta(\mu_1,\sigma_2)\rangle_{n,P} = \langle\delta(\mu_2,\sigma_1)\rangle_{n,P} = \langle\delta(\sigma_1,\sigma_2)\rangle_{n,P} = \epsilon_n\langle\delta(\mu_1,\mu_2)\rangle_{n-1,P} + f_n \tag{19}$$

where

$$\epsilon_n \equiv b_n + 2c_n \tag{20}$$

and

$$f_n \equiv \frac{2a_n - b_n + 1}{3} \tag{21}$$

We shall refer hereafter to the values of the coefficients k_n (where $k_n = a_n,\ b_n,\ c_n,\ d_n,\ \epsilon_n,\ f_n$) evaluated at the critical temperature t_c and at the attractor temperature t_{AF} as k_c and k_{AF} respectively.

4.2 Local Magnetization Profiles

The successive iteration of Eqs. (15) and (3) allow us to obtain, for a fixed P, the local magnetization distribution for both sublattices A and B at any level n for all temperatures. In order to analyse this distribution, it is sufficient to focus on any one of the shortest paths between the two roots R_A and R_B (represented by a broken line in Fig. 1) since all of them are equivalent by symmetry.. Similar to [14,15,16], we identify each site of such a path by a pair (s,l) where l is the level at which the site appeared for

the first time and s is the chemical distance from the site to the root R_A within the level l. These sites can be arranged over the interval $[0,1]$ such that the pair (s,l) corresponds to the point $x \equiv s.3^{-l}$ for a n-level HL (with $l = 1,2,\ldots,n$ and $s = 1,2,4,5,\ldots,3^l - 1$).

In Fig. 6 we show the profiles of the local magnetizations m_{σ_i} versus x for a 7^{th} level HL with $P = 10$ branches at the critical temperature $T_c^{(10)}$ (Fig. 6(a)) and at the attractor temperature $T_{AF}^{(10)}$ (Fig. 6(b)) with the boundary condition $m(x = 0) = 2/3$ (a consequence of $\sigma_{RA} = 0$). Similar profiles are obtained for other values of P ($P > 10$). Notice that positive (negative) magnetizations correspond to sites from the sublattice A (B).

4.3 Multifractality

The magnetization profiles presented in Figure 6 exhibit a highly irregular distribution of magnetizations on the HL, this irregularity being an intrinsic property induced by the fractal topology of the lattice. As we will show, the magnetization profiles have multifractal structures similar to that already reported for the ferromagnetic Ising [14,15,16] and Potts [17] models on HL. In these papers, the multifractality is a characteristic of the system at the critical temperature. Here we have two distinct multifractalities : one at the critical temperature and the other at the whole unusual phase —

these multifractalities being characterized by distinct $f(\alpha)$ spectra.

In order to compute these $f(\alpha)$ spectra, we cover the magnetization profile support at the n-level with boxes of size $l_n = 3^{-n}$ so that within each box there is one spin, which gives origin to the measure in this box. We define the local measure at the i^{th} box, at the n-level HL with P branches, by

$$p_i^{(n)} \equiv \frac{|\, m_{\sigma_i} \,|}{\sum_j |\, m_{\sigma_j} \,|} \qquad (i = 1, 2, \ldots, 3^n + 1) \quad . \tag{22}$$

As the box width goes to zero, or equivalently the HL-level goes to infinity, the measure at the box i scales as $p_i \sim l^{\alpha_i}$ where α_i is the Hölder exponent at this box. In the same limit, the number of boxes N_α with Hölder exponent between α and $\alpha + d\alpha$ scales as $N_\alpha \sim l^{-f(\alpha)}$.

Following the method of Chhabra and Jensen [23.24] we define a set of measures $\{\mu(q,n)\}$, where the measure at the box i is given by

$$\mu_i(q,n) \equiv \frac{[p_i^{(n)}]^q}{\sum_j [p_j^{(n)}]^q} \tag{23}$$

and the $f(\alpha)$ spectrum is achieved by the elimination of the parameter q between

$$f(q) \equiv \lim_{n\to\infty} \frac{\Theta_f(q,n)}{\ln l_n} \tag{24}$$

and

$$\alpha(q) \equiv \lim_{n\to\infty} \frac{\Theta_\alpha(q,n)}{\ln l_n} \tag{25}$$

where

$$\Theta_f(q,n) \equiv \sum_i \mu_i(q,n) \ln \mu_i(q,n) \tag{26}$$

and

$$\Theta_\alpha(q,n) \equiv \sum_i \mu_i(q,n) \ln p_i^{(n)} \quad . \tag{27}$$

In Fig. 7 we show some examples of plots for $P = 10$ that allow us to compute, by measuring the well defined inclination of the straight lines, the $f(q)$ and $\alpha(q)$ variables according to the above definitions. The $f(\alpha)$ spectra for $P = 10$ at the critical and at the AF attractor temperatures are shown in Fig. 8. A detailed analysis near the points where $f(\alpha)$ vanishes shows that $\frac{df(\alpha)}{d\alpha}$ tends to infinity at these points for both temperatures, as usually occurs in deterministic fractals. We can see that at the AF attractor the $f(\alpha)$ spectrum is sharper reflecting the higher homogeneity in the magnetization distribution. Similar spectra are obtained for other values of P ($P > 10$).

We can compute exactly the lowest Hölder exponent α_{min} which is associated with the set of the largest measures, given for large n, by

$$\max_i \left\{ p_i^{(n)} \right\} = \frac{C}{\sum_j \mid m_j \mid} \sim l_n^{\alpha_{min}^{(n)}} \tag{28}$$

where C is a constant independent of n, and $\alpha_{min}^{(n)}$ is the lowest Hölder exponent at the n-level. The denominator $\sum_j \mid m_j \mid$ is related, as we will

see in the next section, to the global order parameter of the system whose critical exponent is, for $P = 10$, $\beta = 0.98\ldots$. Thus, we obtain at the critical temperature t_c

$$\alpha_{min}(t_c) = 1 - \frac{\beta}{\nu} \tag{29}$$

which for $P = 10$ gives the value $0.642\ldots$.

In the AF attractor we can assume the same behavior (Eq. (28)) for the largest measures. The ratio between the largest measures at the two different temperatures (t_c and t_{AF}) leads to

$$\alpha_{min}(t_{AF}) = \alpha_{min}(t_c) + \frac{\ln\left(\frac{1+2(t_{AF}-\alpha_{AF})}{1+2(t_c-\alpha_c)}\right)}{\ln 3} \tag{30}$$

which, for $P = 10$, leads to $\alpha_{min}(t_{AF}) = 0.747\ldots$.

The largest Hölder exponent α_{max} associated with the set of smallest measures can also be calculated in an exact way at the critical temperature. The sites corresponding to the smallest measure at two subsequent levels belong to different sublattices. The local magnetizations at these sites follow a particular set of three recurrent equations which can be derived from Eqs. (15). Assuming that the smallest magnetizations $m_{min}^{(n)}$ and $\Delta_{ij}^{(n)}$ at the n-level vanish at the critical temperature neighborhood like $(\delta t_n)^{\beta_M}$ (where $\delta t_n \equiv \frac{|t_n - t_c|}{t_c}$), the set of recurrent equations for $m_{min}^{(n)}$ furnishes the

following equation for β_M

$$[1 + 2a_c y + (a_c^2 - b_c^2)y^2]\{b_c + [c_c(a_c + b_c) - d_c b_c]y\} -$$

$$-c_c[(a_c - b_c)y^2 - y][(b_c^2 - a_c^2)y - (a_c + b_c)] = 0 \qquad (31)$$

where $y \equiv r_c^{\beta_M}$. Therefore, from the critical behavior of $m_{min}^{(n)}$ and $\sum_j |m_j|$ we obtain that

$$\alpha_{max}(t_c) = 1 + \frac{(\beta_M - \beta)}{\nu} \qquad (32)$$

which, for $P = 10$, leads to the value of 1.250.... These exact results for the limit Hölder exponents are in excellent agreement with those obtained by the direct computation of the $f(\alpha)$ spectra: the relative errors, for $P = 10$, are 0.09%, 0.03% and 0.05% for $\alpha_{min}(t_c)$, $\alpha_{min}(t'_{AF})$ and $\alpha_{max}(t_c)$ respectively. These results exhibit the superiority of this method over the box counting method for computing the $f(\alpha)$ spectrum.

5 Thermodynamical Quantities

Once we have calculated local average quantities, let us proceed in this section to the derivation of the global macroscopic functions.

5.1 Order Parameter

The ordering scheme suggested by MC simulations for the 3-state AF Potts model on a bipartite Bravais lattice is the so called BSS which consists of having predominance of one of the states on the sublattice $\mathcal{A}$ and of the other two states distributed with equal probabilities on the sublattice $\mathcal{B}$. A global order parameter per site describing this type of ordering may be defined [25,26,8] by

$$M = \frac{1}{N_s}\left\{ \mid \sum_{i\subset\mathcal{A}} \langle\delta(\sigma_i,0)\rangle - \sum_{i\subset\mathcal{B}} \langle\delta(\sigma_i,0)\rangle \mid + \mid \sum_{i\subset\mathcal{A}} \langle\delta(\sigma_i,1)\rangle - \sum_{i\subset\mathcal{B}} \langle\delta(\sigma_i,1)\rangle \mid + \right.$$
$$\left. + \mid \sum_{i\subset\mathcal{A}} \langle\delta(\sigma_i,2)\rangle - \sum_{i\subset\mathcal{B}} \langle\delta(\sigma_i,2)\rangle \mid \right\} \quad . \tag{33}$$

The sum over $i \subset \mathcal{A}$ ($i \subset \mathcal{B}$) refers to the sites at the sublattice $\mathcal{A}$ ($\mathcal{B}$) and N_s is the total number of sites on the lattice.

It is easy to show that Eq. (33) applied to the n-level of the HL reduces, due to our symmetry-breaking condition, to

$$M_n^{(P)} = \frac{2D_n^{(P)}}{N_{sn}^{(P)}} \tag{34}$$

with

$$D_n^{(P)} \equiv \sum_{i\subset\mathcal{A}} m_{\sigma_i} - \sum_{i\subset\mathcal{B}} m_{\sigma_i} \tag{35}$$

and

$$N_{sn}^{(P)} = \left(\frac{2P}{3P-1}\right)(3P)^n + \frac{4P-2}{3P-1} \tag{36}$$

where $N_{sn}^{(P)}$ is the number of sites at the n-level HL with P branches. Note that the distinct order parameter proposed by Ono [13] reduces, in our case, to $\zeta_1 = (3/4)M_n$ and $\zeta_2 = 0$ (see Defs. (4.1) of Ref. [13]).

Using the set of recurrent equations (15), one is able to show that $D_n^{(P)}$ also follows a recurrence equation given by

$$D_n^{(P)} - D_{n-1}^{(P)} = P(a_n - b_n)\left[\frac{1}{(a_{n-1} - b_{n-1})} - 2\right](D_{n-1}^{(P)} - D_{n-2}^{(P)}) \quad . \quad (37)$$

Iterating this equation one arrives at the following exact expression for the order parameter per site as function of the temperature (implicit in the parameters a and b)

$$M_n^{(P)} = \left(\frac{N_{s1}^{(P)}}{N_{sn}^{(P)}}\right) M_1^{(P)} + \left[\left(\frac{N_{s1}^{(P)}}{N_{sn}^{(P)}}\right) M_1^{(P)} - \left(\frac{N_{s0}^{(P)}}{N_{sn}^{(P)}}\right) M_0^{(P)}\right] \times$$
$$\times \sum_{i=2}^{n} P^{i-1}\left(\frac{b_i - a_i}{b_1 - a_1}\right) \prod_{j=1}^{i-1}[1 + 2(b_j - a_j)] \quad (38)$$

For a fixed point t^* of the renormalization, and for large n, this expression reduces to

$$M_n^{(P)} = \frac{2(3P-1)(1-t^*)(b^* - a^*)}{3[P(1 + 2(b^* - a^*)) - 1]}\left(\frac{1 + 2(b^* - a^*)}{3}\right)^n \quad (39)$$

where a^* and b^* are the coefficients a_n and b_n calculated at a fixed point t^*. Evaluating this expression at the fixed points we verify that $\lim_{n\to\infty} M_n^{(P)}(t_c^{(P)}) = \lim_{n\to\infty} M_n^{(P)}(t_{AF}^{(P)}) = 0$, which proves the vanishing of the order parameter

per site $M^{(P)}$ for the whole range of temperatures, namely

$$M^{(P)}(t) \equiv \lim_{n\to\infty} M_n^{(P)}(t) = 0 \qquad \frac{-1}{2} \leq t \leq 0, \quad \forall\, P \geq 10 \quad . \qquad (40)$$

In Fig. 9 we show, for $P = 10$, the behavior of the order parameter per site $M_n^{(10)}$ as function of temperature for different levels of the HL, exhibiting an abrupt decay as the level n increases.

Although $M_n^{(P)}$ vanishes in the thermodynamical limit for all temperatures, let us show that it exists a non-null critical exponent $\beta^{(P)}$. First of all, we verified (see, for $P = 10$, Fig. 10) that, for a fixed temperature T, $M_n^{(P)}$ behaves as :

$$M_n^{(P)}(T) \sim A(T,P) L_n^{-\theta(T,P)} \qquad (41)$$

where $L_n = 3^n$ is the linear size of the n-level HL with P branches, $A(T,P)$ is a finite constant (which becomes $0.717\ldots$ for $T = T_c$ and $P = 10$), and $\theta(T,P)$ is a temperature dependent exponent ($\theta(T,P) \geq 0$; $\theta(T_c,10) \simeq 0.357$, $\theta(T_{AF},10) \simeq 0.253$).

Besides that, we have also observed (see Fig. 11) that the inflexion point $T_n^{*(P)}$ (where $\partial^2 M_n^{(P)}/\partial T^2 \,|_{T_n^{*(P)}} = 0$) approaches $T_c^{(P)}$ as $n \to \infty$ according to :

$$\delta T_n^{(P)} \equiv \frac{T_n^{*(P)} - T_c^{(P)}}{T_c^{(P)}} \sim A^*(P) L_n^{-\zeta(P)} \qquad (42)$$

where $A^*(10) \simeq 0.413$ and $\zeta(10) \simeq 0.369 \simeq (2.71)^{-1}$. As the plot of Fig.

11 refers to $9 \leq n \leq 17$ and $\frac{1}{\zeta(10)}$ differs from $\nu^{(10)}$ by only 1.5%, we expect that this discrepancy vanishes in the thermodynamical limit. A similar fact happens for other values of $P > 10$ and we can consider that

$$\zeta(P) = \frac{1}{\nu^{(P)}} \tag{43}$$

where $\nu^{(P)}$ has the value obtained in Fig. 4 for the correlation length critical exponent. $T_n^{*(P)}$ plays, therefore, the role of the rounding temperature which appears in the finite size scaling theory (see, e.g., [27]) as the temperature at which the plot of a given quantity for a finite size departs significantly from the corresponding thermodynamical limit.

Combining expressions (41), (42) and (43) we obtain the following asymptotic behavior for $M_n^{(P)}$ in the neighborhood of T_c :

$$M_n^{(P)}(T_n^{*(P)}) \sim B(P)(\delta T_n^{(P)})^{\beta^{(P)}} \tag{44}$$

where the numerical estimate for $\beta^{(P)}$ is

$$\beta^{(P)} = \nu^{(P)}\theta(T_c^{(P)}, P) \tag{45}$$

which gives for $P = 10$ the approximate value of 0.982. Combining Eq. (44) with the recursive equation for $D_n^{(P)}$ (Eq. (37)) we obtain the following exact value for $\beta^{(P)}$

$$\beta^{(P)} = \frac{\ln\left[\frac{3}{1+2(t_c-c_c)}\right]}{\ln r_c^{(P)}} \qquad (\beta^{(10)} = 0.982\ldots) \tag{46}$$

which agrees very well with the numerical estimate (Eq. (45)). In Fig. 4 we show the plot of the exact value of $\beta^{(P)}$ as function of $d_f^{(P)}$. The asymptotic behavior of β in the neighborhood of d_c is $\beta^{(P)} \sim [0.342\ldots](d_f(P) - d_c)^{-0.387\ldots}$.

5.2 Internal Energy and Specific Heat

The calculation of the internal energy of the n-level HL with P branches involves, according to Eq. (1), the thermal average of $\delta(\sigma_i, \sigma_j)$ over all the spins at the n-level. Since this average is the same for all bonds (Eq. (19)), it follows that the dimensionless internal energy per bond at the n-level $E_{bn}^{(P)}$ is given by

$$E_{bn}^{(P)} = \frac{\langle \mathcal{H}_n^{(P)} \rangle_{n,P}}{3 \mid J_n^{(P)} \mid N_{bn}^{(P)}} = \langle \delta(\sigma_i, \sigma_j) \rangle_{n,P} \qquad (47)$$

where $N_{bn}^{(P)}$ is the number of bonds in the n-level HL with P branches. $E_{bn}^{(P)}$ satisfies (see Eq. (19)) the following recurrence equation :

$$E_{bn}^{(P)} = \epsilon_n E_{bn-1}^{(P)} + f_n \qquad . \qquad (48)$$

Successive iterations of the above equation leads to the following exact expression for the dimensionless internal energy per site in the fractal limit

$$E_s^{(P)} \equiv \lim_{n\to\infty} \frac{\langle \mathcal{H}_n^{(P)} \rangle_{n,P}}{3 \mid J_n^{(P)} \mid N_{sn}^{(P)}} = \frac{(3P-1)}{2P} \left(\sum_{i=1}^{\infty} f_i \prod_{j=i+1}^{\infty} \epsilon_i + f_\infty \right) \qquad . \qquad (49)$$

The plots of $E_s^{(P)}$ as functions of temperature are shown, for $P = 10$ and $P = 27$, in Fig. 12. Notice that, in the $T \to \infty$ limit where all the configurations are equiprobable, the asymptotic value of $E_s^{(P)}$ reduces to the expected answer

$$\lim_{n\to\infty} \langle \delta(\sigma_i, \sigma_j) \rangle_{n,P} \left(\frac{N_{bn}^{(P)}}{N_{sn}^{(P)}} \right) = \frac{1}{3} \left(\frac{3P-1}{2P} \right) \quad . \tag{50}$$

The dimensionless specific heat per bond at the n-level HL with P branches $C_{bn}^{(P)}$ defined by

$$C_{bn}^{(P)} \equiv \frac{1}{3k_B N_{bn}^{(P)}} \frac{\partial \langle \mathcal{H}_n^{(P)} \rangle_{n,P}}{\partial T} \tag{51}$$

can be obtained by differentiating the recurrence for $E_{bn}^{(P)}$ (Eq. (48)), which provides a recursive equation for $C_{bn}^{(P)}$. After successive iterations of this equation we obtain the following expression for the dimensionless specific heat per site in the fractal limit

$$\begin{aligned} C_s^{(P)} \equiv & \lim_{n\to\infty} \frac{1}{3k_B N_{sn}^{(P)}} \frac{\partial \langle \mathcal{H}_n^{(P)} \rangle_{n,P}}{\partial T} = \\ & \left(\frac{3P-1}{2P} \right) \left\{ \sum_{i=3}^{\infty} \left[\epsilon_i' \left(\sum_{l=1}^{i-2} f_l \prod_{j=l+1}^{i-1} \epsilon_j + f_{i-1} \right) + f_i' \right] \prod_{k=i+1}^{\infty} \epsilon_k z_k + \right. \\ & \left. + \epsilon_\infty' \left(\sum_{i=1}^{\infty} f_i \prod_{j=i+1}^{\infty} \epsilon_j + f_\infty \right) + f_\infty' \right\} \end{aligned} \tag{52}$$

where

$$\epsilon_i' \equiv \frac{|J_i| \partial \epsilon_i}{k_B \partial T} \quad , \quad f_i' \equiv \frac{|J_i| \partial f_i}{k_B \partial T} \quad , \quad z_i \equiv \frac{J_i}{J_{i-1}} \quad . \tag{53}$$

In Fig. 13 we show, for $P = 10$ and $P = 27$, the plots of the specific heat per site as functions of temperature. The maximum of the specific heat occurs at a temperature $T_{max}^{(P)}$ lower than the critical temperature $T_c^{(P)}$. A similar behavior is found in the $q = 3$ anisotropic Potts model with ferromagnetic and antiferromagnetic interactions in the two respective directions of the square lattice [28] (whose ground state degeneracy is infinite) and in the F model of an antiferroeletric [29] (which exhibits an unconventional type infinite-order transition).

Assuming a critical behavior for the energy in the neighborhood of the critical temperature like $E_{bn}^{(P)} \sim (\delta t_n^{(P)})^{a^{(P)}}$ the recurrent equation (48) leads to the following exact expression for the specific heat critical exponent $a^{(P)}$

$$a^{(P)} = 1 - \sigma^{(P)} = 1 + \frac{\ln \epsilon_c}{\ln r_c^{(P)}} \quad . \tag{54}$$

On the other hand, it follows from the definition of $\epsilon_c^{(P)}$ as function of $t_c^{(P)}$ (see Eqs. (18) and (20)) and from Eq. (3) that

$$r_c^{(P)} = 3P\epsilon_c^{(P)} \quad . \tag{55}$$

Combining Eqs. (1), (5), (54) and (55) we derive that

$$d_f(P)\nu^{(P)} = 2 - a^{(P)} \tag{56}$$

which proves that the hyperscaling law for Bravais lattices continues to be valid (replacing the spatial dimension by the fractal one) for the whole

family of HL's considered herein. Such law has already been numerically verified for the ferromagnetic Ising [30,16] and Potts models [17] on a number of HL's.

Although there is no proof that the scaling laws valid for Bravais lattices continue to hold for fractals, if we assume that the Rushbrooke scaling relation (which, in fact, has been verified for the Ising ferromagnet on the Wheatstone-bridge HL [31]) and the Fisher one are valid for the considered family of HL's then one would obtain a value for the η critical exponent at t_c which is different from $\eta_{AF}^{(P)}$ shown in Fig. 4. This would lead a discontinuity of η at the critical temperature (for example, for $P = 10$, $\eta_c \simeq -0.38$ and $\eta_{AF} \simeq -0.51$).

5.3 Entropy

In order to calculate the entropy in an exact way, let us use another method (see for example [32]) which is based on 'restricted partition functions' defined by

$$Z_{F_n}^{(P)} \equiv Tr\left[\delta(\sigma_{RA}, \sigma_0)\delta(\sigma_{RB}, \sigma_0)\exp\left(-\beta\mathcal{H}_n^{(P)}(\sigma)\right)\right] \qquad (\sigma_0 = 0, 1, 2) \quad (57)$$

and

$$Z_{AF_n}^{(P)} \equiv Tr\left[\delta(\sigma_{RA},\sigma_0)\delta(\sigma_{RB},\sigma_1)\exp\left(-\beta\mathcal{H}_n^{(P)}(\sigma)\right)\right] \qquad (\sigma_0,\sigma_1 = 0,1,2;\ \sigma_0 \neq \sigma_1) \quad . \tag{58}$$

The partition function $Z_n^{(P)}$ at the n-level of the HL with P branches is, thus, given by

$$Z_n^{(P)} = 3Z_{AF_n}(2+\lambda_n) \tag{59}$$

with $\lambda_n \equiv Z_{F_n}^{(P)}/Z_{AF_n}^{(P)}$. One can easily derive the following recurrent equations :

$$Z_{AF_{n+1}}^{(P)} = [Z_{AF_n}^{(P)}]^{3P}\left[3(1+\lambda_n+\lambda_n^2)\right]^P \qquad (Z_{AF_0}^{(P)} = 1) \tag{60}$$

$$\lambda_{n+1} = \left[\frac{2+6\lambda_n+\lambda_n^3}{3(1+\lambda_n+\lambda_n^2)}\right]^P \qquad (\lambda_0 = \exp(3J_n^{(P)}/k_BT)) \tag{61}$$

whose iteration leads to

$$\lim_{n\to\infty}\frac{\ln Z_n^{(P)}}{N_{sn}^{(P)}} = \frac{(3P-1)}{2}\sum_{i=0}^{\infty}\frac{\ln[3(1+\lambda_i+\lambda_i^2)]}{(3P)^{i+1}} \quad . \tag{62}$$

Eq. (62) allow us to derive the following exact expression for the dimensionless entropy per site $S_s^{(P)}$ in the fractal limit

$$S_s^{(P)}(T) \equiv \lim_{n\to\infty}\frac{S_n^{(P)}}{k_BN_{sn}} = \frac{(3P-1)}{2}\sum_{i=0}^{\infty}\frac{1}{(3P)^{i+1}}\left\{\ln\left[3(1+\lambda_i+r_i^2)\right] - \right.$$
$$\left. -\lambda_i\ln\lambda_i\left(\frac{1+2\lambda_i}{1+\lambda_i+r_i^2}\right)\right\} \tag{63}$$

where $S_n^{(P)} = k_B[\ln Z_n^{(P)} + T\frac{\partial \ln Z_n^{(P)}}{\partial T}]$. In Fig. 14 we show the behavior of the entropy as function of temperature for $P = 10$: the plot of $S_s^{(27)}$ is

indistinguishable from that of $S_s^{(10)}$ within the scale used in this figure. It is worth pointing out that the entropy is continuous at T_c, as expected from the absence of latent heat (due to the continuity of $C_s^{(P)}$ at $T_c^{(P)}$, as we can see from Fig. 13) and from the continuity of the order parameter at the critical temperature. This fact shows that the transition is continuous. The residual entropy s_0 is :

$$s_0^{(P)} = S_s^{(P)}(T=0) = \frac{(3P-1)}{2} \sum_{i=0}^{\infty} \frac{\ln[3(1+\lambda_i+\lambda_i^2)]}{(3P)^{i+1}} \qquad (64)$$

and for $P = 10$ has the value 0.5496..., which corresponds to approximately 50% of the entropy at the $T \to \infty$ limit ($S_s(T=\infty) = \ln 3$). Notice that this is a relatively big value if we compare it with the $q = 3$ AF Potts model on the simple cubic lattice where $s_0 \simeq 0.34 S_s(T \to \infty)$ [26].

6 Conclusions

We present an exactly soluble model defined in a family of diamond hierarchical lattices which has an unusual phase like that one suggested by Berker and Kadanoff for complex systems with non-zero residual entropy per spin. In this phase, the pair correlation function decays algebraically with a temperature independent η exponent. We calculate, in an exact way, the multifractal local magnetizations and a number of thermodynam-

ical functions together with their corresponding critical exponents.

We prove that the order parameter vanishes for all range of temperatures. We believe that the vanishing of the order parameter along the unusual phase is due mainly to the multiplicity of spin configurations which generates a tendency towards equiprobability for the three states.

We also proved the hyperscaling law for the studied family of fractals.

As far as we know, there has been no report in the literature concerning : i) **exact** calculations of any thermodynamical quantity along the mentioned unusual phase, in particular, of the order parameter; ii) the **temperature dependence** of the $f(\alpha)$ spectrum characterizing the multifractality of the local average magnetizations : the $f(\alpha)$ calculated at the critical temperature differs from that at the unusual phase; iii) the **discontinuity** at the critical temperature of the critical exponent η, which was derived assuming that certain scaling laws continue to hold for this family of fractal systems.

Finally, we would like to point out the found similarities and differences between the studied system and the ferromagnetic XY model on the square lattice (see, e.g., [33,34]). The similarities are : i) the algebraic decay of correlations along the low-temperature phase; ii) the vanishing of the order parameter; iii) the absence of divergence in the specific heat. The differences are : i) in the XY model η varies continuously with the temperature.

while in our family of systems, if the scaling laws are valid. η jumps to a different value at T_c; ii) the correlation length ξ diverges, as T_c is approached from above, as an exponential law in the XY model in contrast to the power law obtained in the considered fractal family; iii) the peak of the specific heat in the XY model occurs above the critical temperature, contrarily to what happens in the studied family of systems. As the considered fractal family is somewhat similar to the bidimensional XY model, it would be interesting to look for a certain type of topological excitations, the vortices, which at low temperatures occur for the XY model in tightly bound pairs that unbind at the critical temperature. Although these vortices were initially defined for a continuous spin model, Kolafa [35] extended them to the 3-state Potts antiferromagnet. The search for these vortices in the considered family of HL's would require the use of another technique, like for example Monte Carlo simulations, since the symmetry breaking condition used in our recursive method does not allow us to distinguish the state 1 from the state 2.

Acknowledgements

We acknowledge Constantino Tsallis for useful remarks. We thank the Brazilian agency Conselho Nacional de Desenvolvimento Científico e Tecnológico (CNPq) for financial support.

Figure Captions

- **Figure 1**: First steps of construction of the studied diamond type HL with $P = 10$ branches. $G^{(0)}$, $G^{(1)}$ and $G^{(2)}$ are the corresponding graphs obtained at the respective levels $n = 0, 1, 2$. The sites of the sublattice $\mathcal{A}$ ($\mathcal{B}$) are represented by circles (squares) and, in particular, the open circle (open square) is the root R_A (R_B). The broken line at $n = 2$ indicates an arbitrary shortest path joining the roots.

- **Figure 2**: The renormalized transmissivities t' as functions of t and the corresponding flow diagrams for the studied HL with $P = 9, 10$ and 27 branches. The circle and the square stand for the unstable (critical point) and stable (attractor) respective fixed points. By succesive iterations, an initial value $t^{(P)}$ where $-1/2 \leq t^{(P)} < t_c^{(P)}$ and $P > P_c = 9.25\ldots$ will converge to the attractor of the unusual phase $t_{AF}^{(P)}$. Another initial transmissivity $t^{(P)}$ with $t_c^{(P)} < t^{(P)} \leq 0$ will converge to the attractor of the paramagnetic phase $t_f^{(P)} = 0$.

- **Figure 3**: The fixed points t^* at the critical temperature $t_c^{(P)}$ (represented by triangles) and at the attractor temperature $t_{AF}^{(P)}$ of the unusual phase (represented by squares) as functions of the fractal dimension $d_f^{(P)}$ of the diamond type HL with P branches. The lines are

guides for the eye.

- **Figure 4**: The critical exponents of the correlation length $\nu^{(P)}$ (represented by small circles) and of the order parameter $\beta^{(P)}$ (represented by squares), as well as the correlation function exponent $\eta_{AF}^{(P)}$ for the whole unusual phase (represented by triangles) versus the fractal dimension $d_f^{(P)}$. The lines are guides for the eye.

- **Figure 5**: (a) Pictorial representation of the graph $G^{(n)}$ corresponding to the n level of the considered HL with P branches. $G^{(n)}$ is the union of the subgraph $G_1^{(n)}$ (whose edges are represented by broken lines), which contains the spins σ_1 and σ_2 created at the n-level and the spins μ_1 and μ_2 generated at previous levels, and of the subgraph $G_2^{(n)}$ which contains, besides μ_1 and μ_2, the remaining spins including the spin σ_{R_A} at the root R_A (represented by Ξ) which is fixed at the state 0. In (b) $G_2^{(n)}$ has been replaced by an effective graph $G_{ef}^{(n)}$ whose effective dimensionless Hamiltonian is given by Eq. (14).

- **Figure 6**: The local magnetizations $m_o^{(A)}$ and $m_e^{(B)}$ of the spins along a shortest path between the roots R_A and R_B of the HL with $P = 10$ branches at the $n = 7$ level versus the position x. (a) and (b) were calculated at the critical temperature T_c and at the attractor temper-

ature T_{AF} respectively. The positive magnetizations $m_n^{(A)}$ correspond to spins belonging to the sublattice $\mathcal{A}$ and the negative ones $m_n^{(B)}$ refer to those of the sublattice $\mathcal{B}$.

- **Figure 7**: The respective sums $\Theta_f(q,n)$ and $\Theta_o(q,n)$ defined in Eqs. (26) and (27) versus the level n of the HL with $P = 10$ branches for different values of q. These sums were calculated at $T = T_c$; similar straight lines are obtained for $T = T_{AF}$.

- **Figure 8**: The $f(\alpha)$ spectra at the critical temperature T_c (represented by circles) and at the attractor temperature T_{AF} (represented by triangles) for $P = 10$. The lines are guides for the eye.

- **Figure 9**: The order parameter per site $M_n^{(10)}$ as function of temperature for consecutive levels n, $3 \leq n \leq 11$, of the HL with $P = 10$ branches. $T_c^{(10)}$ and $T_{AF}^{(10)}$ correspond, respectively, to the critical and attractor temperatures in the $n \to \infty$ limit.

- **Figure 10**: The logarithm of the order parameter per site $M_n^{(10)}$ for the HL with $P = 10$ branches versus n calculated at $T = T_c^{(10)}$ (represented by points) and $T = T_{AF}^{(10)}$ (represented by triangles).

- **Figure 11**: The logarithm of the relative difference between the in-

flexion point temperature of $M_n^{(10)}$ and the critical temperature $T_c^{(10)}$ versus n for the HL with $P = 10$ branches. The straight line corresponds to the best square fitting.

- **Figure 12**: The dimensionless internal energy per site $E_s^{(P)}$ of the HL's with $P = 10$ (full line) and $P = 27$ (broken line) branches as functions of temperature. $T_c^{(10)}$ and $T_c^{(27)}$ correspond to their respective critical temperatures.

- **Figure 13**: The dimensionless specific heat per site $C_s^{(P)}$ of the HL's with $P = 10$ (full line) and $P = 27$ (broken line) branches as functions of temperature.

- **Figure 14**: The dimensionless entropy per site $S_s^{(P)}$ of the HL with $P = 10$ branches (the curves for $P = 10$ and $P = 27$ are indistinguishable in the used scale) versus temperature. $s_0^{(P)}$ is the residual entropy per site ($s_0^{(10)} \simeq 0.5496$ and $s_0^{(27)} \simeq 0.5493$) and $\ln 3$ is the expected asymptotic value for $S_s^{(P)}(T \to \infty)$.

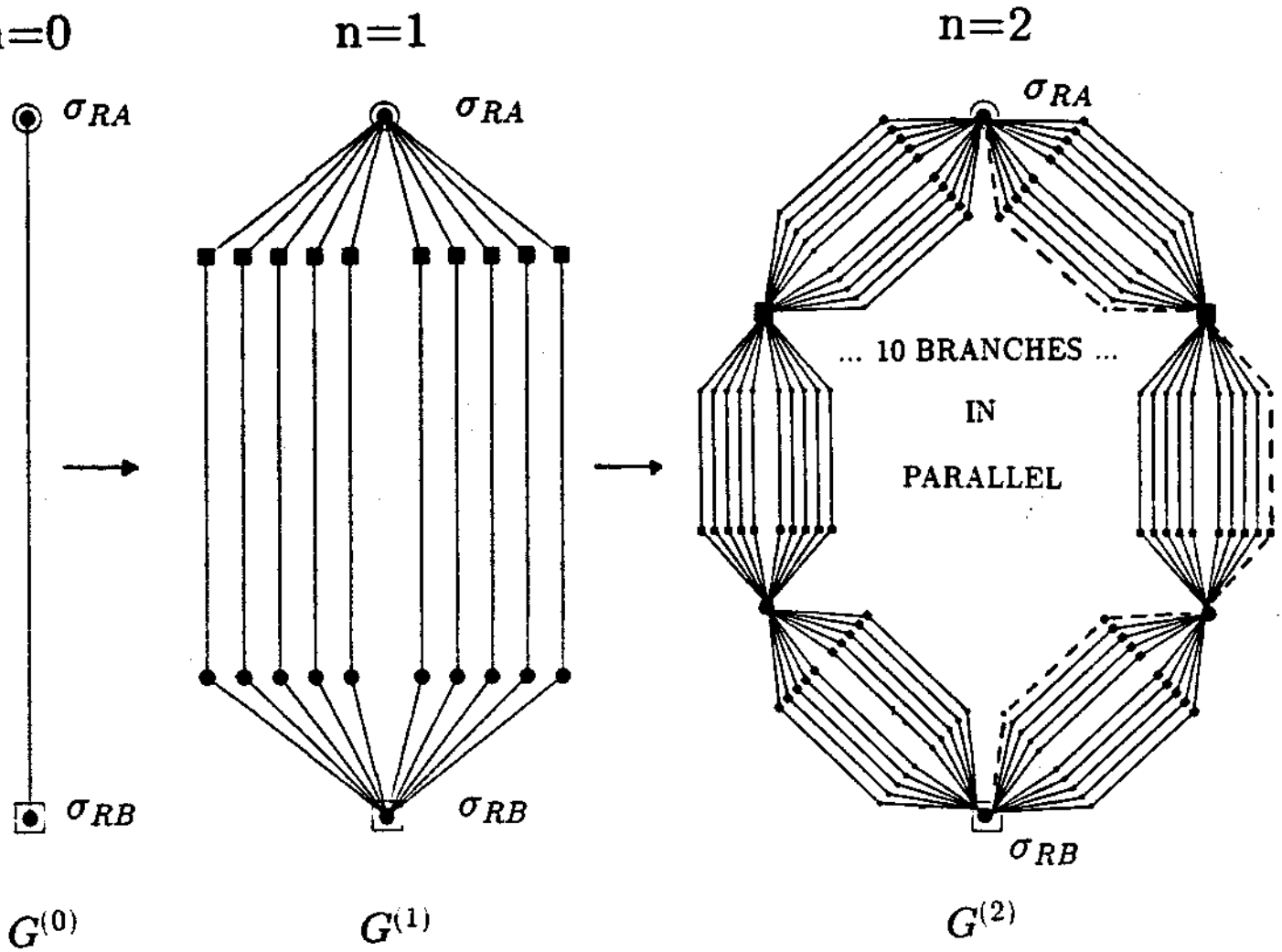

FIGURE 1

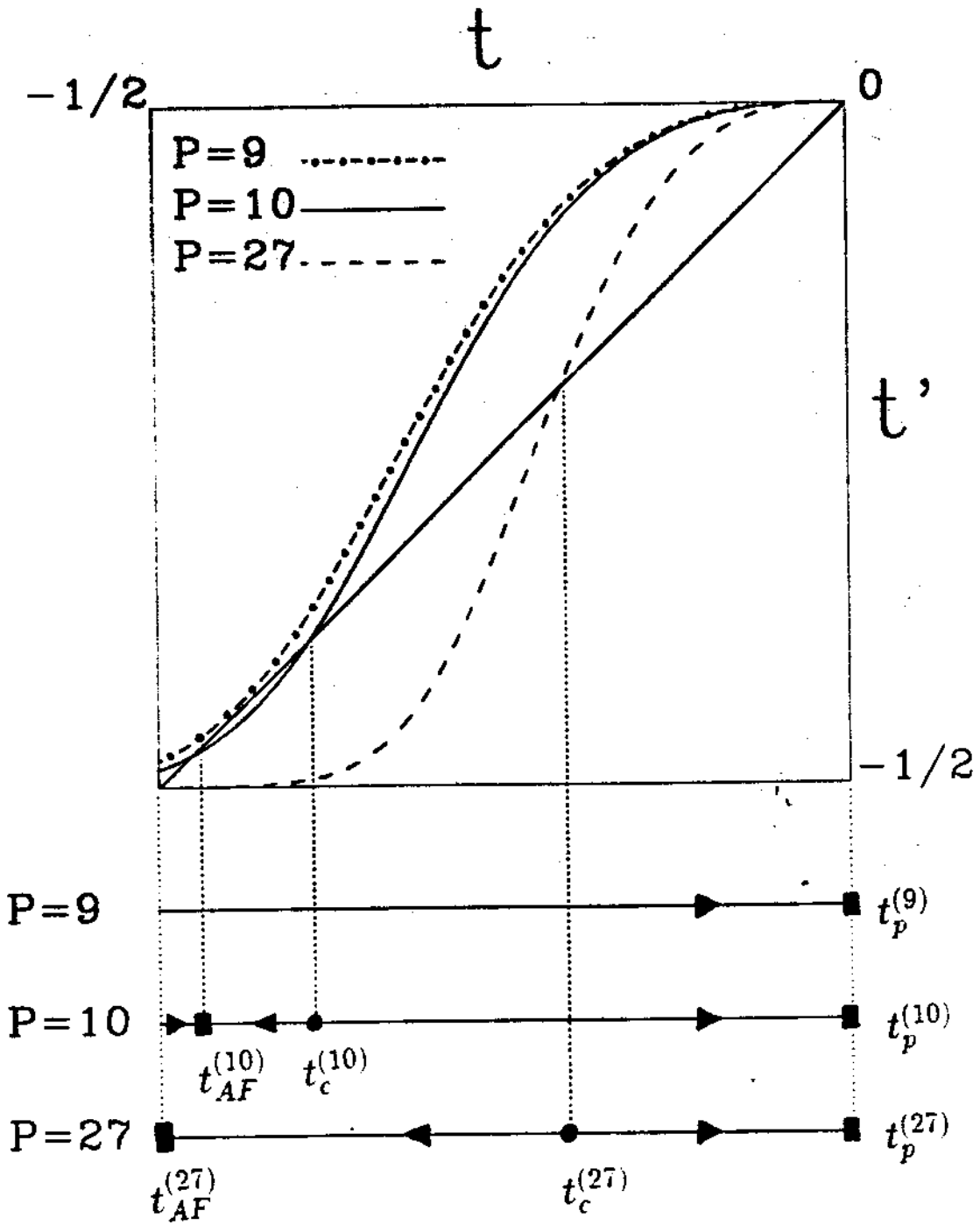
t
−1/2
0
P=9
P=10
P=27
t'
−1/2
P=9
$t_p^{(9)}$
P=10
$t_p^{(10)}$
$t_{AF}^{(10)}$
$t_c^{(10)}$
P=27
$t_p^{(27)}$
$t_{AF}^{(27)}$
$t_c^{(27)}$

FIGURE 2

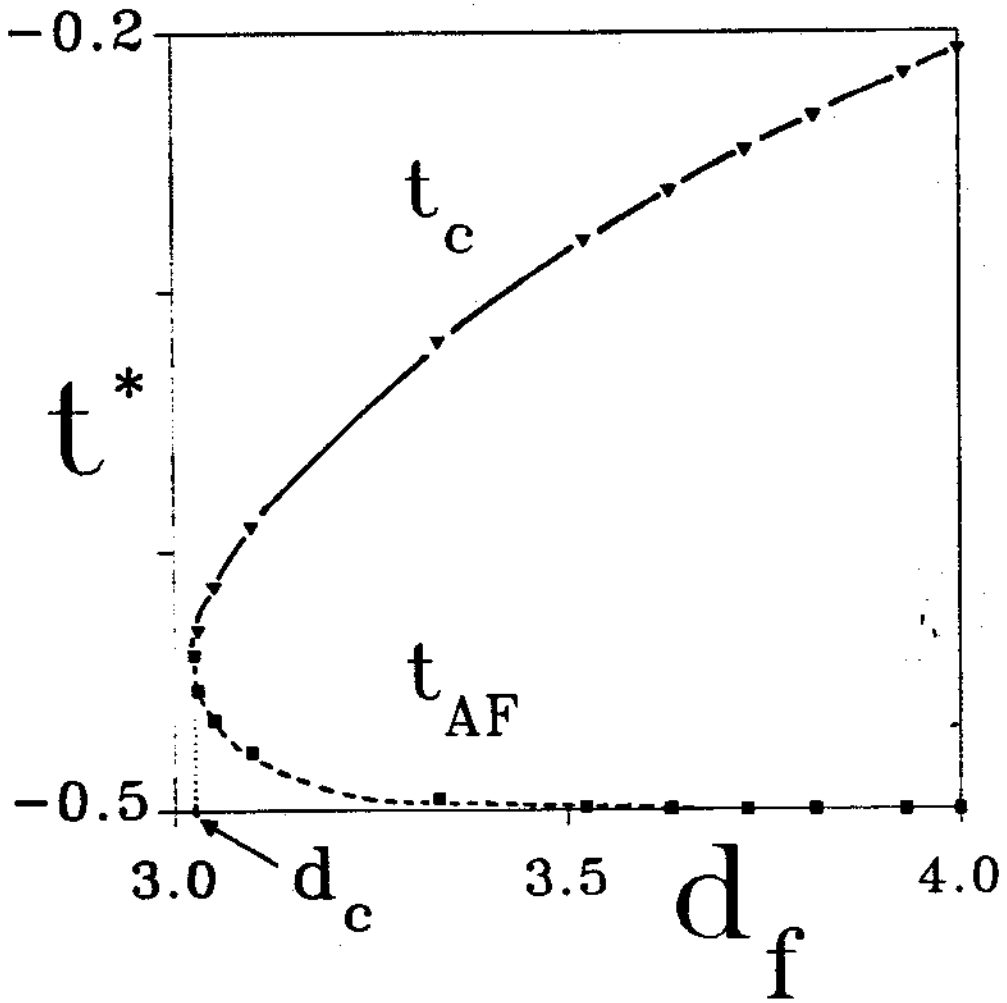

FIGURE 3

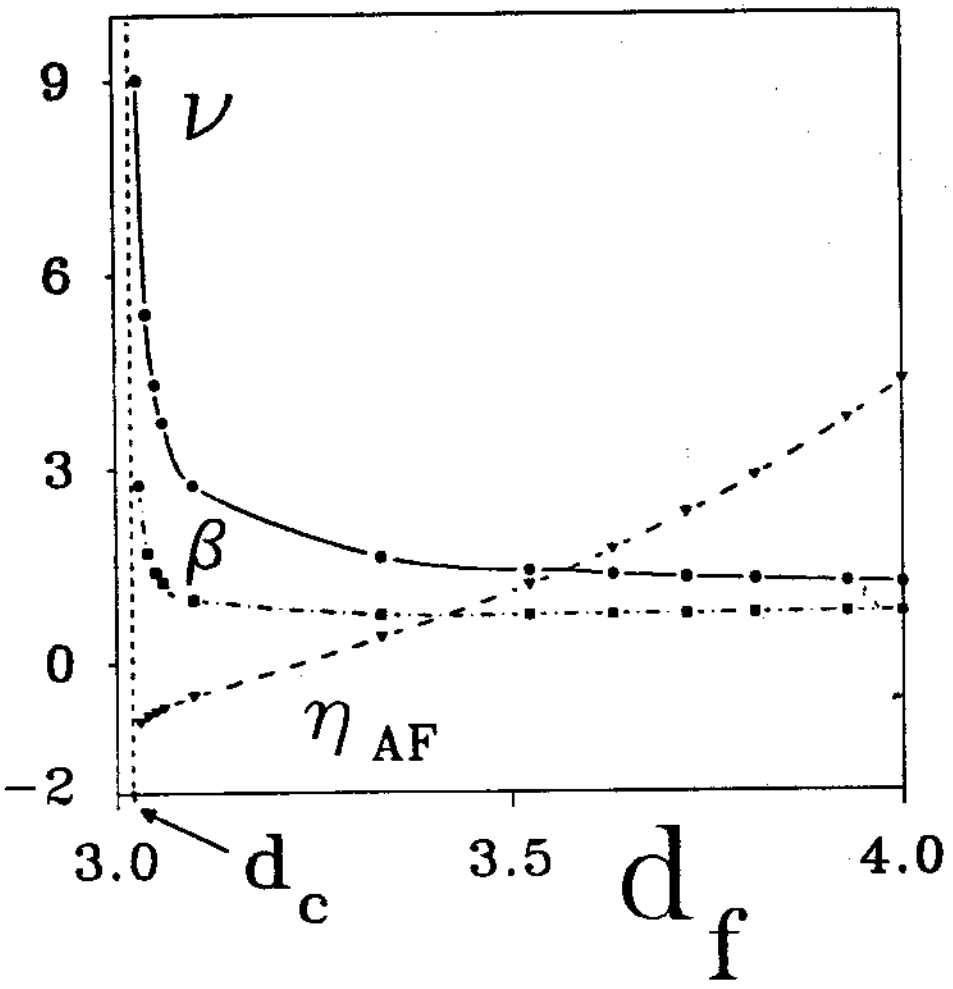

FIGURE 4

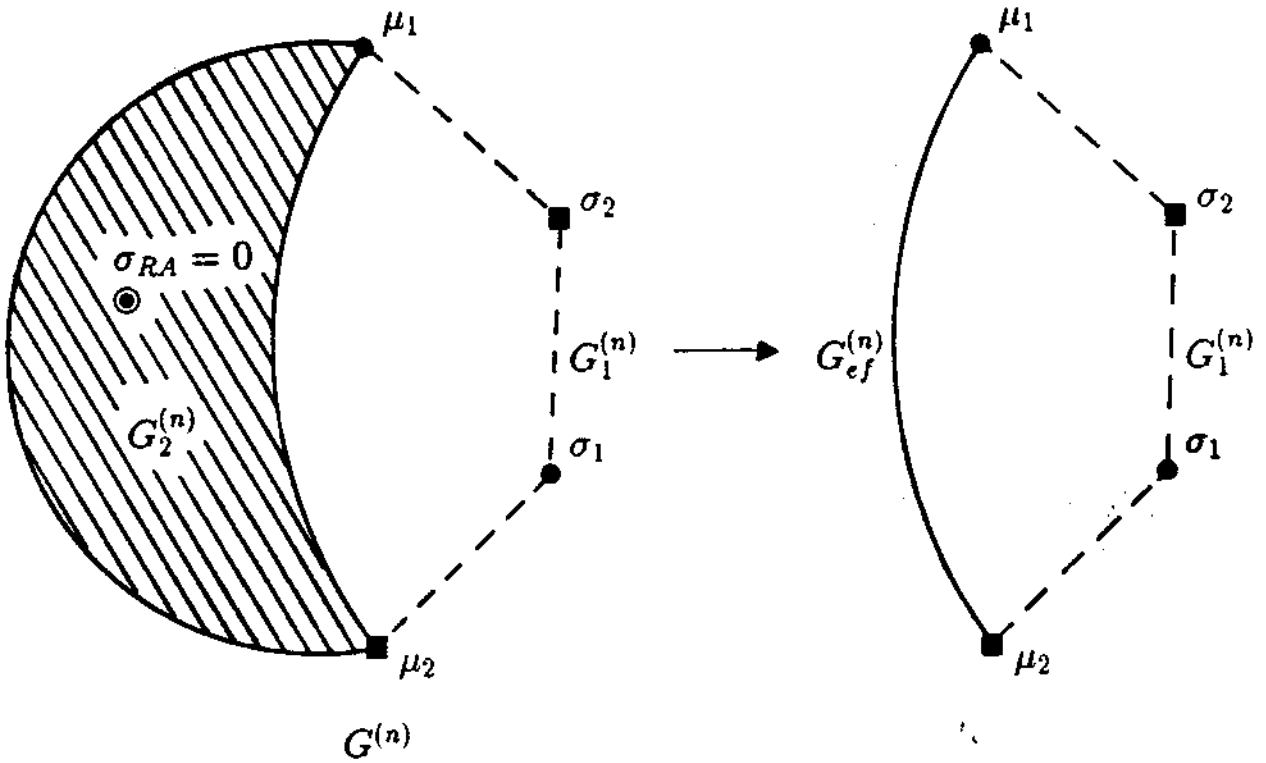

5 (a) 5 (b)

FIGURE 5

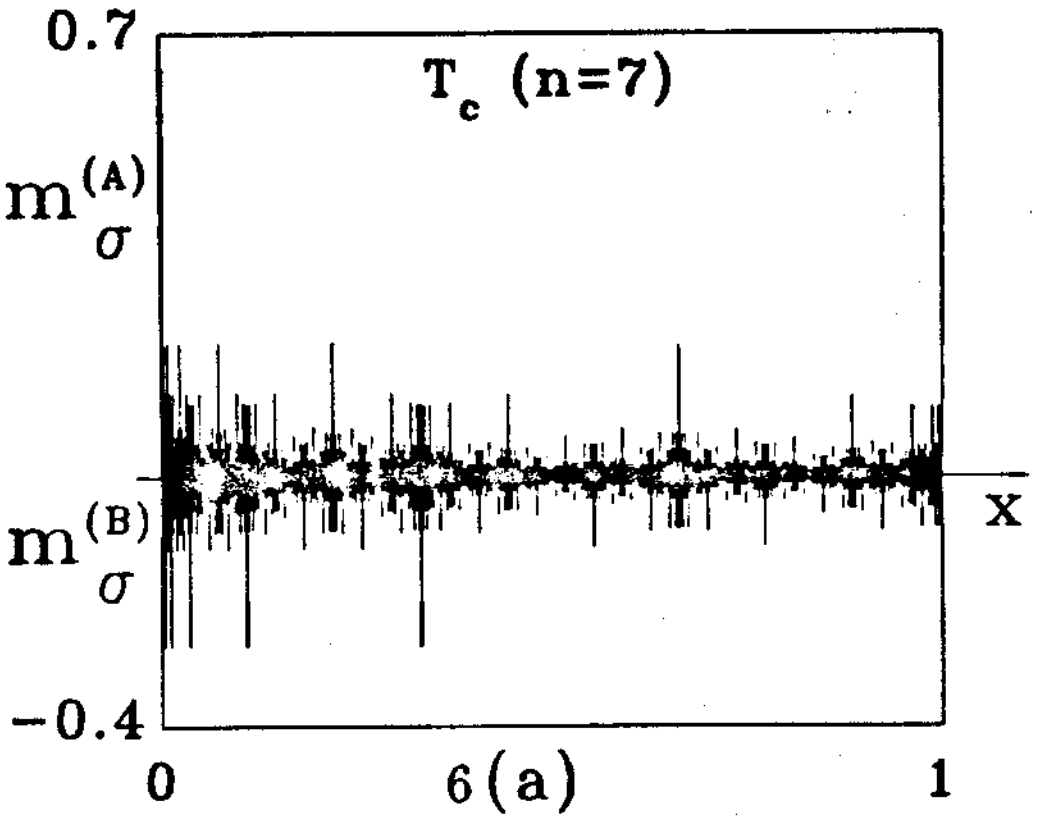
0.7
T_c (n=7)
$m_\sigma^{(A)}$
$m_\sigma^{(B)}$
x
-0.4
0
6(a)
1

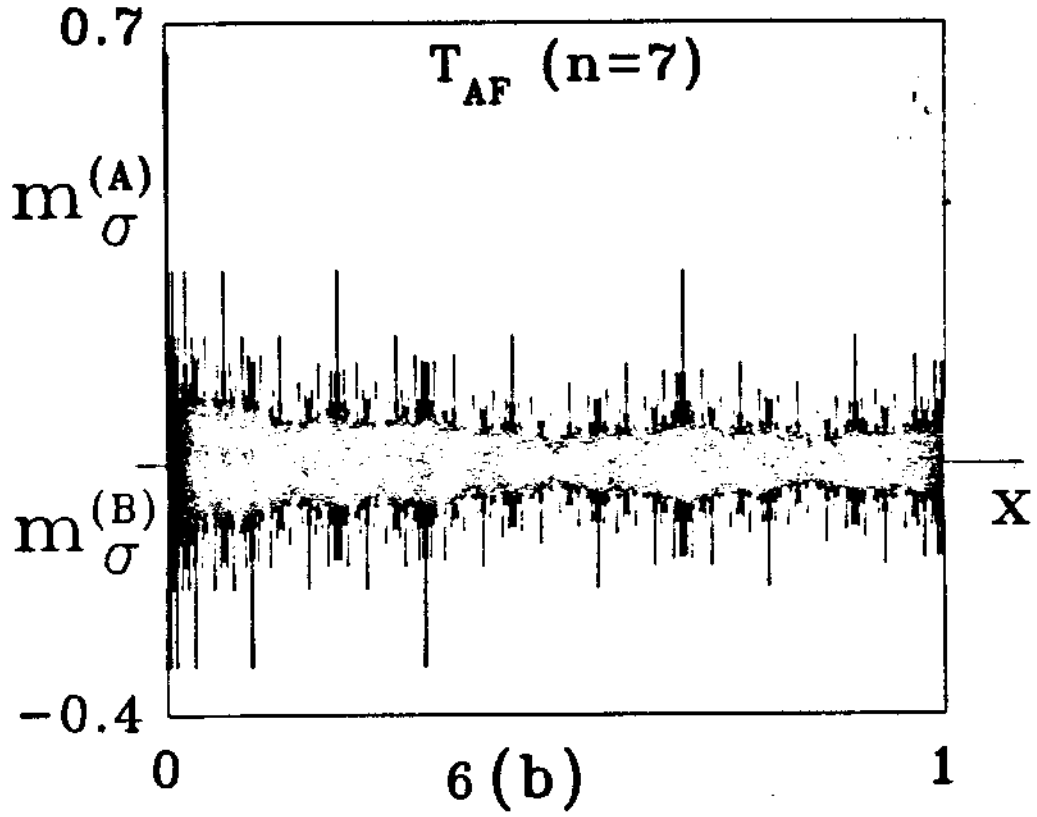
0.7
T_{AF} (n=7)
$m_\sigma^{(A)}$
$m_\sigma^{(B)}$
x
-0.4
0
6(b)
1

FIGURE 6

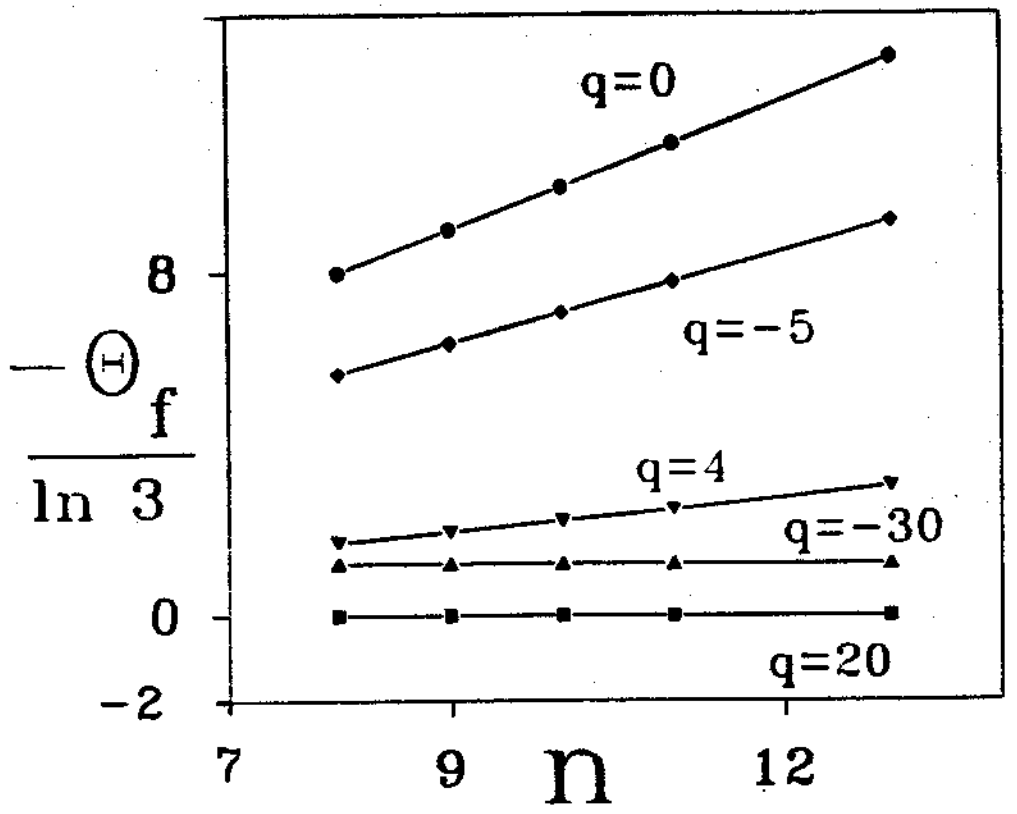

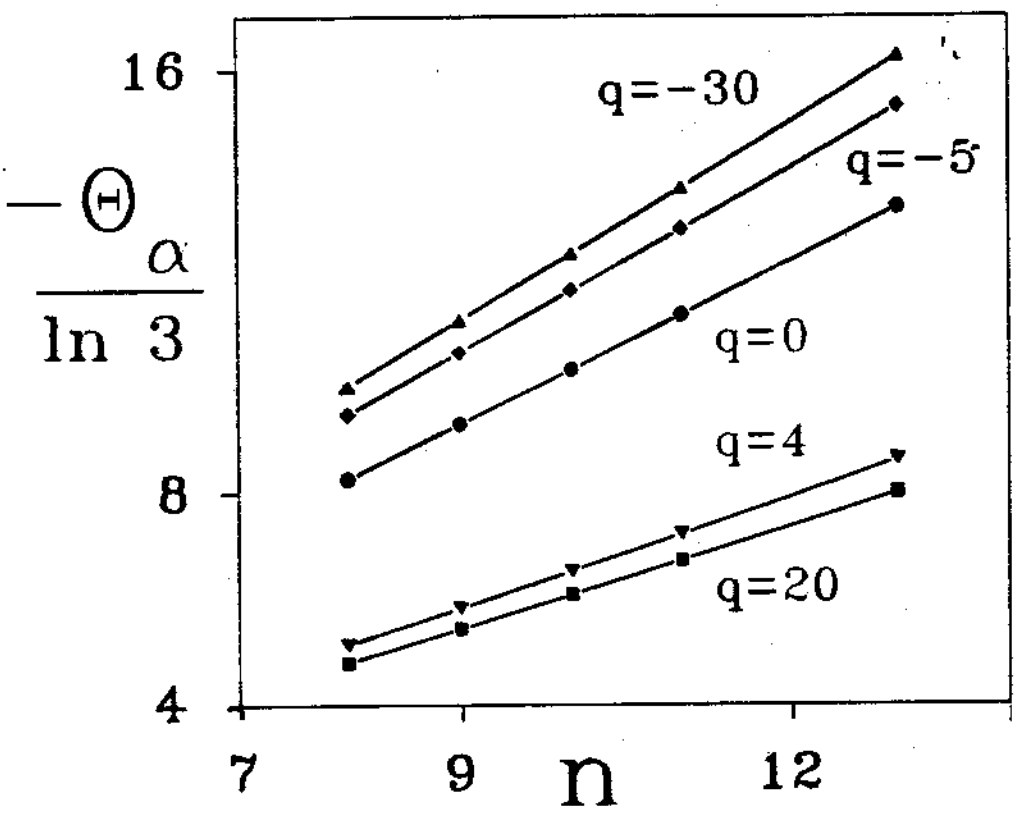

FIGURE 7

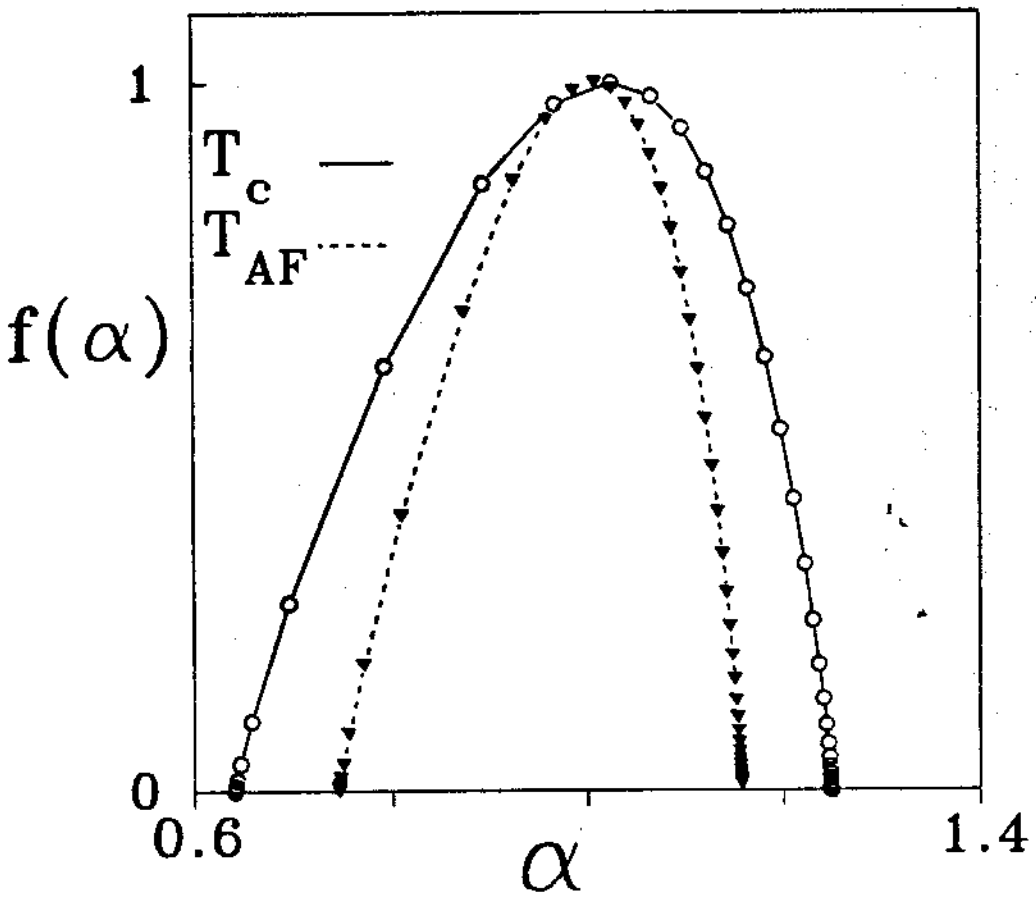

FIGURE 8

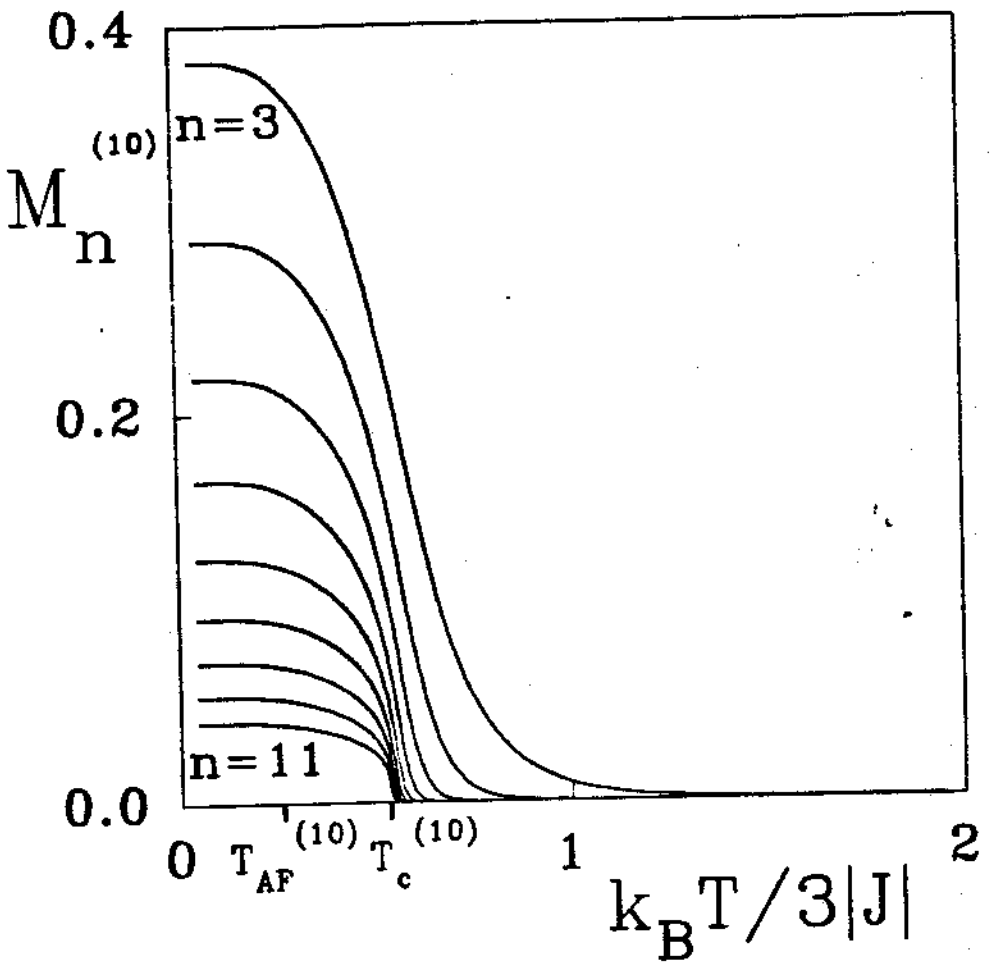

FIGURE 9

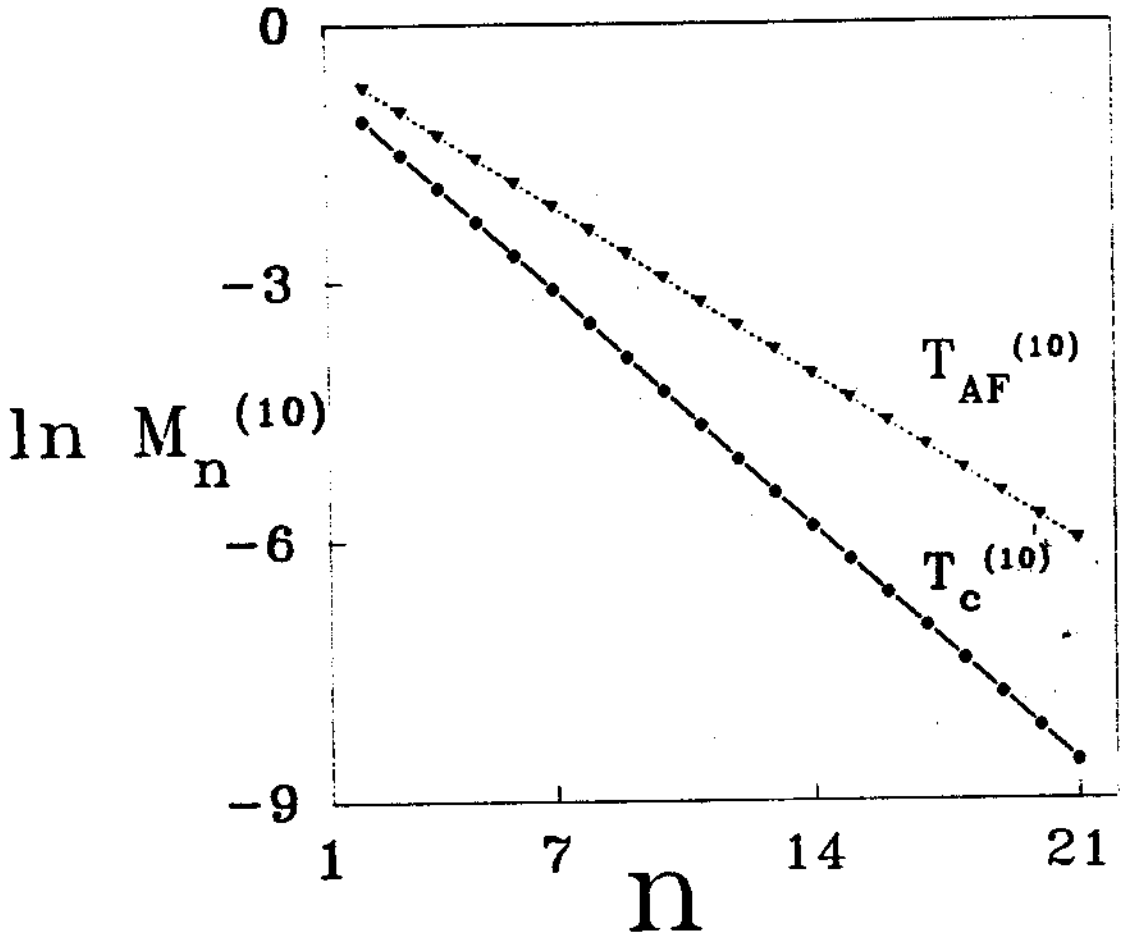

FIGURE 10

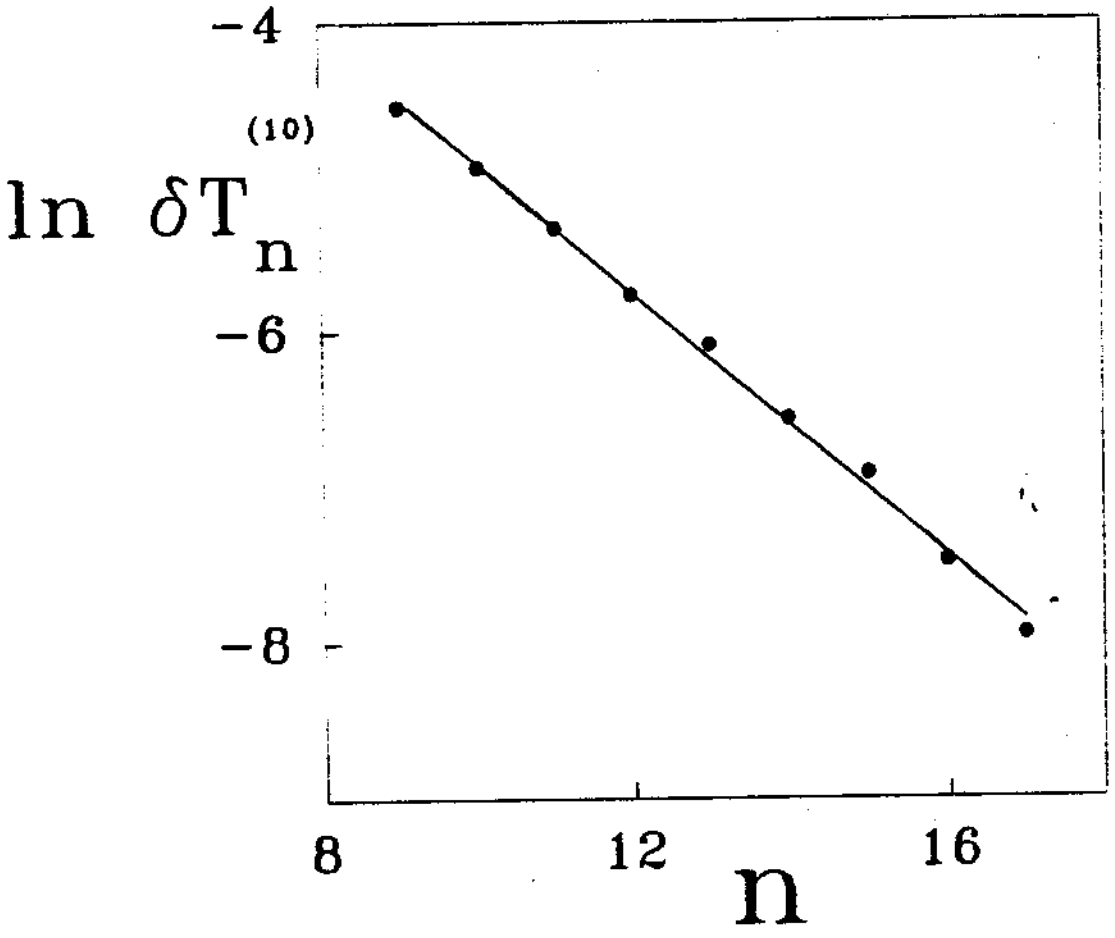

FIGURE 11

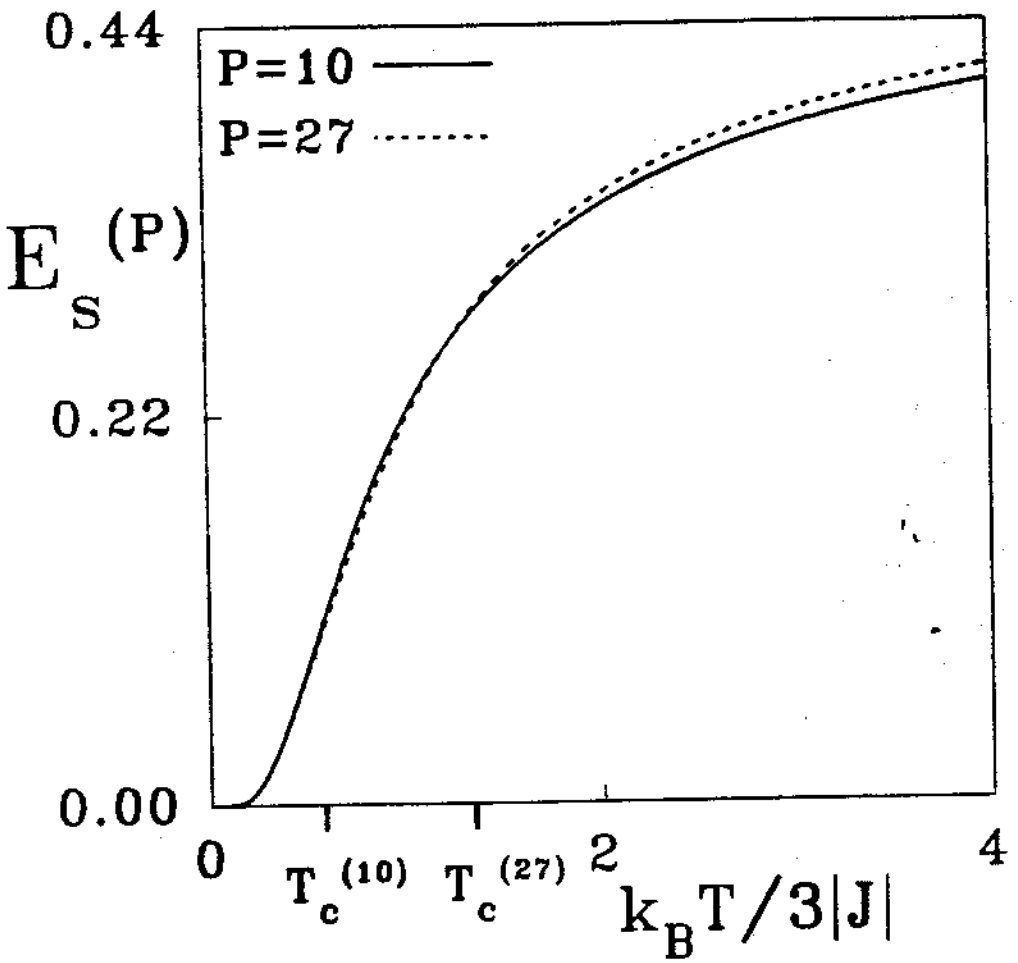

FIGURE 12

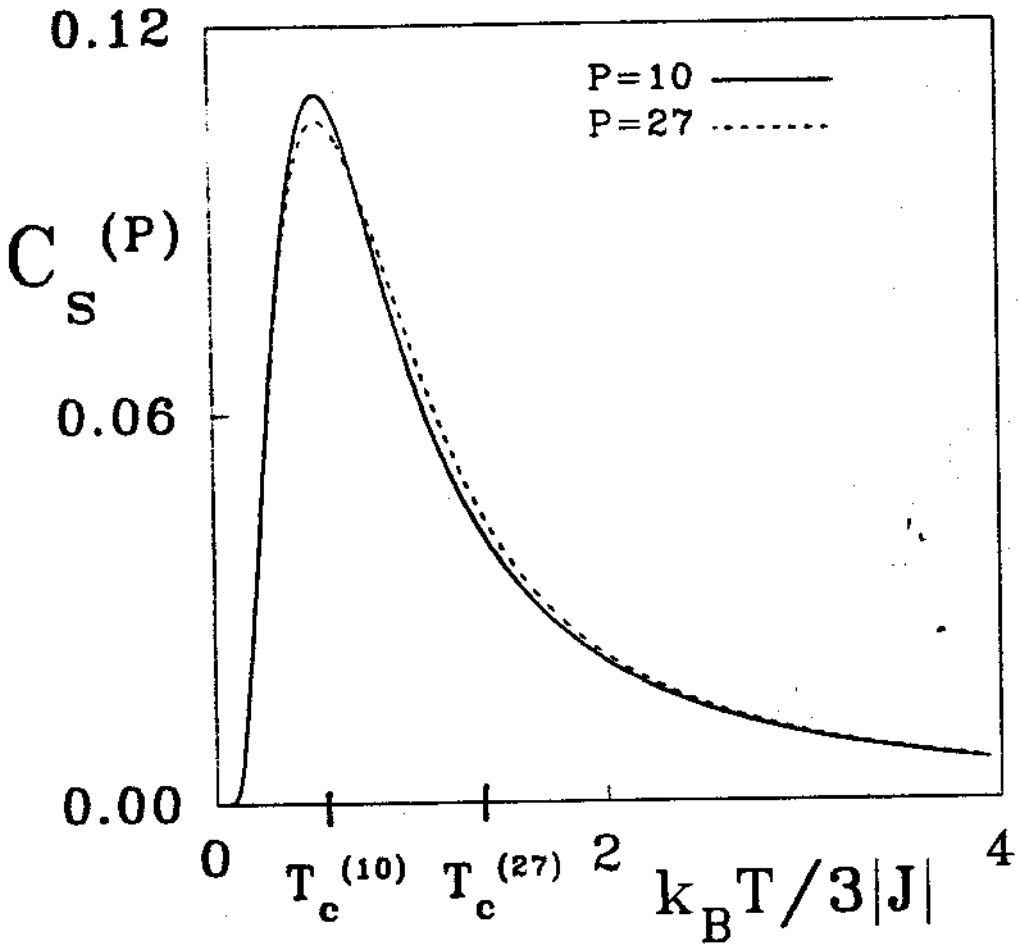

FIGURE 13

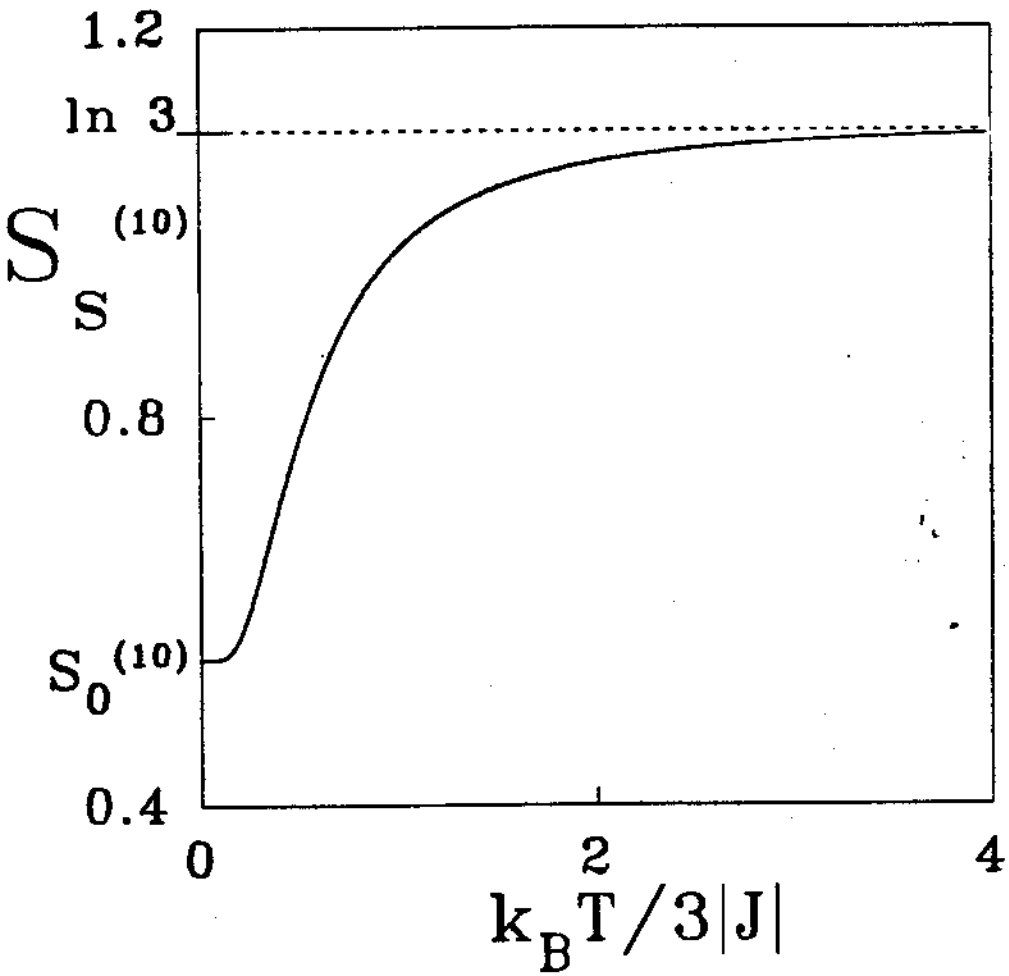

FIGURE 14

References

[1] E. H. Lieb, Phys. Rev. B 162, 162 (1967)

[2] G. H. Wannier, Phys. Rev. 79, 357 (1950)

[3] K. Binder and A. P. Young, Rev. Mod. Phys. 58, 801 (1986)

[4] A. V. Bakaev, V. I. Kabanovich and A. M. Kurbatov, J. Phys. A 25, L31 (1992)

[5] Y. Chow and F. Y. Wu, Phys. Rev. B 36, 285 (1987)

[6] A. N. Berker and L. P. Kadanoff, J. Phys. A 13, L259 (1980)

[7] Z. Rácz and T. Vicsek, Phys. Rev. B 27, 2992 (1983)

[8] J. S. Wang, R. H. Swendsen and R. Kotecký, Phys. Rev. B 42, 2465 (1990)

[9] R. Riera, J. Phys. A 19, 3395 (1986)

[10] A. Bakchick, A. Benyoussef and N. Boccara, J. Phys. C 3, 1727 (1991)

[11] Y. Qin and Z. R. Yang, Phys. Rev. B 43, 8576 (1991)

[12] F. S. de Menezes and A. C. N. de Magalhães, Phys. Rev. B 46, 11642 (1992)

[13] I. Ono, Prog. Theo. Phys. Suppl. 87, 102 (1986)

[14] W. A. M. Morgado, S. Coutinho and E. M. F. Curado, J. Stat. Phys. 61, 913 (1990)

[15] W. A. M. Morgado, S. Coutinho and E. M. F. Curado, Revista Brasileira de Fisica 21, 247 (1991)

[16] S. Coutinho, O. D. Neto, J. R. L. de Almeida, E. M. F. Curado and W. A. M. Morgado, Phys. A 185, 271 (1992)

[17] L. da Silva, E. M. F. Curado, W. A. M. Morgado and S. Coutinho (to be published)

[18] J. R. Melrose, J. Phys. A 16, 3077 (1983)

[19] J. W. Essam and C. Tsallis, J. Phys. A 19, 409 (1986)

[20] C. Tsallis and S. V. F. Levy, Phys. Rev. Lett. 47, 950 (1981)

[21] F. Y. Wu, Rev. Mod. Phys. 54, 235 (1982)

[22] A. C. N. de Magalhães and J. W. Essam, J. Phys. A 19, 1655 (1986)

[23] A. Chhabra and R. V. Jensen, Phys. Rev. Lett. 62, 1327 (1989)

[24] A. B. Chhabra, C. Meneveau, R. V. Jensen and K. R. Sreenivasan, Phys. Rev. A 40, 5284 (1989)

[25] J. R. Banavar, G. S. Grest and D. Jasnow, Phys. Rev. Lett. 45, 1424 (1980)

[26] B. Hoppe and L. L. Hirst, J. Phys. A 18, 3375 (1985)

[27] M. N. Barber, in *Phase Transitions and Critical Phenomena* Vol. 8, p. 145, edited by C. Domb and J. L. Lebowitz (Academic Press, New York, 1983)

[28] W. Kinzel, W. Selke and F. Y. Wu, J. Phys. A 14, L399 (1981)

[29] E. H. Lieb and F. Y. Wu, in *Phase Transitions and Critical Phenomena* Vol.1, p. 331, edited by C. Domb and M. S. Green (Academic Press, New York, 1972)

[30] C. Tsallis, J. Phys. C 18, 6581 (1985)

[31] E. P. da Silva and C. Tsallis, Phys. A 167, 347 (1990)

[32] P. M. Bleher and E. Zalys, Commun. Math. Phys. 120, 409 (1989)

[33] J. M. Kosterlitz, J. Phys. C 7, 1046 (1974)

[34] J. E. V. Himbergen and S. Chakravarty, Phys. Rev. B 23, 359 (1981)

[35] J. Kolafa, J. Phys. A 17, L777 (1984)